Gravitational wave generation in a viable scenario of inflationary magnetogenesis

Ramkishor Sharma,[1,*] Kandaswamy Subramanian,[1,†] and T. R. Seshadri[2,‡]
[1]*IUCAA, Post Bag 4, Pune University Campus, Ganeshkhind, Pune—411007 India*
[2]*Department of Physics & Astrophysics, University of Delhi, New Delhi—110007 India*

(Received 27 December 2019; accepted 5 May 2020; published 21 May 2020)

Generation of magnetic fields during inflation is a promising mechanism for the origin of the observed large scale magnetic fields in the universe. Among several attempts, a popular model is one where the inflaton and the electromagnetic field are coupled through a coupling function f leading to a term in the Lagrangian density of the form, $f^2F^{\mu\nu}F_{\mu\nu}$. A number of potential difficulties with such models have been raised in the literature. In our earlier work, we have suggested viable models of inflationary magnetogenesis which avoid these problems and at the same time can lead to either nonhelical or helical magnetic fields of astrophysical interest. Our models require a low energy scale for inflation and reheating (reheating temperature, $T_R < 10^4$ GeV) and generate a blue spectrum of electromagnetic (EM) field which peaks around the horizon scale of reheating. We show here that the anisotropic stress associated with these EM fields naturally source the production of a stochastic background of Gravitational waves (GW) with frequencies in the range of tens of nano Hertz to milli Hertz. These two extremes of the range can be probed respectively by pulsar timing arrays (PTA) experiments and the upcoming Laser Interferometric Space Array (LISA). The peak value of the GW spectrum energy represented by $d\Omega_{\rm GW}/d\ln k$ is 10^{-6} for the models which lead to nonhelical primordial fields and 2×10^{-6} for the helical case for $T_R = 100$ GeV. In this case the spectrum peaks at a frequency 30 μHz for nonhelical case and at 40 μHz for helical case. These values are obtained when the ratio of EM energy density to the cosmological density at reheating $\epsilon \sim 1$ and decrease approximately as ϵ^2 for smaller values. The amplitude is similar for a lower value of T_R, but the frequency at which the GW spectrum peaks decreases as T_R. The gravitational waves generated are unpolarized if the EM fields are nonhelical but are circularly polarized for helical primordial fields. If detected in the future these gravitational waves will provide a unique probe of such models of inflationary magnetogenesis.

DOI: 10.1103/PhysRevD.101.103526

I. INTRODUCTION

The discovery of gravitational waves by LIGO and VIRGO detectors from binary black hole and neutron star black hole binary mergers [1–5] opened a new era in astronomy. Gravitational waves (GW) can even probe sources which are not detectable through electromagnetic radiation like black hole mergers. Primordial GW can be used to probe various epochs in the early Universe. One of these epochs is the inflationary era during which the universe underwent a rapid accelerated expansion. The inflationary framework provides a solution to several problems in standard cosmology like horizon and flatness problems [6]. It also gives a natural explanation for the origin of initial density fluctuations [7,8] which are later amplified via gravity to form large-scale structures in the universe. Tensor perturbations (gravitational waves) are also produced in a manner similar to that of scalar density perturbations during inflation [9,10]. These tensor perturbations travel freely after generation as their interaction with the rest of the fluid is very weak. Since, the energy scale at which inflation took place is not known, the present observations only put an upper bound on this scale of inflation from the nondetection of tensor perturbations in the cosmic microwave background radiation [11].

There are various other epochs in the early universe where the production of GW could have taken place. These include the production of GW from braneworlds [12,13], topological defects [14], phase transitions [15–33], reheating [34–36], and primordial turbulence [37–40]. Gravitational waves may be represented by the transverse traceless (TT) part of the metric perturbations. They are sourced by the corresponding TT part of the energy momentum tensor. Indeed any process which generates an anisotropic stress can produce GW. This can happen, for

*ramkishor@iucaa.in
†kandu@iucaa.in
‡trs@physics.du.ac.in

example, if magnetic fields are generated during phase transition or during inflation.

In this paper, we focus on the production of the gravitational waves from the primordial magnetic fields which are generated during inflation. Magnetic fields have been observed over a wide range of scales in the universe [41–45]. These fields are assumed to be generated by the amplification of seed fields via flux freezing evolution followed by a turbulent dynamo mechanism [46]. A number of scenarios of generation of seed magnetic fields have been suggested in literature such as generation during inflation [47–68], phase transitions [69–72], recombination, reionization and structure formation [73–77]. The importance of inflationary scenarios of magnetic field generation as against other mechanisms lies in the fact that the former gives a natural way of generating fields coherent on large length scales. A popular model for such generation is one where one couples a time dependent function to the usual electromagnetic (EM) action. In particular Ratra [48] model takes the Lagarangian density of the form $f^2F^{\mu\nu}F_{\mu\nu}$ where f is a function of inflaton field and $F_{\mu\nu}$ the electromagnetic field tensor. Although this model generates magnetic fields of sufficient strength to satisfy a number of observational constraints, it suffers from the backreaction and strong coupling problems [78]. Another potential difficulty for such magnetogenesis scenarios arises due to charged particle production by the Schwinger mechanism which arrests the growth of magnetic field [79].

In a recent study by Sharma *et al.* [80], we have suggested a scenario in which these problems can be circumvented at the cost of having a low scale inflation. In this model, the coupling function f increases during inflation starting from an initial value of unity and becomes very large at the end of inflation. Such an evolution of f is free from the above mentioned problems. However, the coupling between the charges and EM field becomes very small at the end. To get back the standard EM theory we introduced a transition in the evolution of f immediately after the end of inflation during which time it decreases back to unity at reheating and after that f becomes constant. During this postinflationary era both electric and magnetic energy density increase. By demanding that EM energy density should remain below the background energy density, we obtained a bound on reheating and inflationary scales. Our models can generate both nonhelical and helical magnetic fields and satisfy known observational constraints. They predict a blue spectrum for the magnetic field energy density peaked at small length scales, typically a fraction of the Hubble radius at reheating [80,81]. The generated field energy density can also be a significant fraction of the energy density of the Universe at those epochs.

The anisotropic stress associated with such primordial EM fields lead to a stochastic gravitational wave background. The process is to a certain degree similar to that which obtains during a first order phase transitions in the early Universe. Prior to reheating, the electric energy density was nonzero and its amplitude is typically greater than the magnetic energy density. Hence, prior to reheating, both electric and magnetic fields contribute to the anisotropic stress and result in GW production with a dominant contribution from the electric field. Electric fields are however damped out after reheating due to the very large conductivity of the universe. Thus after reheating only the generated magnetic fields contribute to the generation of stochastic GW. This interplay between electric and magnetic field both contributing to stochastic GW leads to a characteristic feature in the GW energy spectrum. We calculate here the strength of the stochastic GW background generated for several of our inflationary magnetogenesis models. The predicted signals are compared with the sensitivity of the future space based gravitational waves detector like the Laser Interferometer Space Antenna (LISA) or for some reheating scales limits obtained from Pulsar Timing Arrays (PTA).

The paper is organized as follows. In Sec. II we set up the general formalism for describing the evolution of the stochastic GW energy spectrum in terms of the tensor perturbation of the metric. We also introduce the different bases for representing the GW energy spectrum depending upon the nature of the source of these tensor perturbations. In Sec. III, we study the inflation generated electromagnetic fields as the source of these perturbations and derive expressions for the resulting anisotropic stress needed to calculate the GW energy spectrum. The predicted stochastic GW spectrum due to nonhelical electromagnetic fields is calculated in Sec. IV A. The helical case is considered in Sec. IV B. We also compare these predictions with expected limits from LISA and PTA experiments. Detection of the generated GW spectrum with LISA is discussed in Sec. V. Some of the details of the calculations are left to several appendices. The last section contains a discussion of our results and conclusions.

II. STOCHASTIC GRAVITATIONAL WAVES: STANDARD FORMALISM

Gravitational waves may be represented by the transverse-traceless part of the space-time metric perturbation. These are sourced by the TT part of the energy momentum tensor. In the context of this paper, such TT component of the energy-momentum tensor is provided by the EM field. In this section we set up the general formalism to describe the evolution of stochastic GW energy spectrum in the expanding universe so that in subsequent sections, we can calculate the gravitational waves produced by the inflation generated EM field in our scenario. For this, we follow Caprini *et al.* [22] and Caprini *et al.* [82]. We consider a homogeneous, isotropic and a spatially flat background

expanding universe. The metric for such a universe with tensor perturbation is,

$$ds^2 = a^2(\eta)(-d\eta^2 + (\delta_{ij} + 2h_{ij})dx^i dx^j).$$

Here η is the conformal time, x^i represents the comoving coordinates for the space dimensions, $a(\eta)$ is the scale (or expansion) factor and h_{ij} represents the tensor perturbations of the metric, in the transverse and traceless gauge. The energy density of the stochastic GW in terms of these tensor perturbations can be expressed as [29],

$$\rho_{\rm GW} = \frac{1}{16\pi G}\frac{\langle h'_{ij}h'^{ij}\rangle}{a^2}. \tag{1}$$

Here $h^{ij} = \delta^{im}\delta^{jn}h_{mn}$, prime ($'$) denotes the derivative with respect to conformal time and $\langle\rangle$ represents ensemble average. We define the Fourier transformation of the tensor perturbations as

$$h_{ij}(\vec{k},\eta) = \int d^3x h_{ij}(\vec{x},\eta)e^{-i\vec{k}\cdot\vec{x}},$$

with the corresponding inverse transform defined as,

$$h_{ij}(\vec{x},\eta) = \int \frac{d^3k}{(2\pi)^3} h_{ij}(\vec{k},\eta)e^{i\vec{k}\cdot\vec{x}},$$

where we use the symbol h_{ij} for both the real space and Fourier space components. The Fourier components $h_{ij}(\vec{k},\eta)$ satisfy,

$$k^i h_{ij} = 0 \quad \text{and} \quad h^i_i = 0.$$

In Fourier space, $\rho_{\rm GW}$ can be expressed as

$$\rho_{\rm GW} \equiv \int d\ln k \frac{d\rho_{\rm GW}}{d\ln k} = \frac{1}{16\pi G a^2}\int \frac{d^3k}{(2\pi)^3}\int \frac{d^3q}{(2\pi)^3}\langle h'_{ij}(\vec{k},\eta)h'^{*}_{ij}(\vec{q},\eta)\rangle e^{i(\vec{k}-\vec{q})\cdot\vec{x}}. \tag{2}$$

We will refer to $d\rho_{\rm GW}/d\ln k$ as the GW energy spectrum. To estimate the energy density in GW, we need to know how h_{ij} evolves with time. The evolution of h_{ij} is governed by the Einstein equation, using which, we get the following linearized equation of motion for h_{ij} in presence of a source,

$$h''_{ij} + \frac{2a'}{a}h'_{ij} + k^2 h_{ij} = 8\pi G a^2 \bar{T}_{ij}. \tag{3}$$

Here $a^2\bar{T}_{ij}$ is the transverse traceless part of the energy-momentum tensor of the source. In our work, we consider both nonhelical as well as helical EM field as the source of gravitational waves. The convenient basis for expressing the solution to the GW equation depends on whether the GW is linearly or circularly polarized depending on whether we consider nonhelical or helical EM fields respectively as the source.

The basis set suitable to represent the linear polarization of the gravitational waves are [29],

$$e^T_{ij} = \frac{1}{\sqrt{2}}(\hat{e}^1\times\hat{e}^1 - \hat{e}^2\times\hat{e}^2)_{ij}$$
$$e^\times_{ij} = \frac{1}{\sqrt{2}}(\hat{e}^1\times\hat{e}^2 + \hat{e}^2\times\hat{e}^1)_{ij}.$$

Here $(\hat{e}^1, \hat{e}^2, \hat{e}^3 \text{ or } \hat{k})$ are a set of mutually orthonormal basis vectors of our coordinate system, "×" represents a tensor product and we assume that gravitational waves propagates in the $\hat{e}^3$ or $\hat{k}$ direction in this coordinate system. These basis vectors satisfy the following properties to ensure the transverse traceless nature of the tensor perturbations,

$$\hat{k}^i e^{(T,\times)}_{ij} = 0, \qquad \delta^{ij}e^T_{ij} = 0,$$
$$e^{(T,\times)}_{ij}e^{(\times,T)ij} = 0, \qquad e^{(T,\times)}_{ij}e^{(T,\times)ij} = 1.$$

The GW tensor perturbation in terms of this basis is,

$$h_{ij}(\vec{k},\eta) = h^T(\vec{k},\eta)e^T_{ij} + h^\times(\vec{k},\eta)e^\times_{ij} \tag{4}$$

Further, the suitable basis for representing the circular polarization of the gravitational waves are [82],

$$e^\pm_{ij} = -\frac{1}{2}(\hat{e}^1 \pm i\hat{e}^2)_i \times (\hat{e}^1 \pm i\hat{e}^2)_j.$$

Here $e^\pm_{ij}$ satisfy the following properties,

$$\hat{k}^i e^\pm_{ij} = 0, \qquad \delta^{ij}e^\pm_{ij} = 0, \qquad e^\pm_{ij}e^{\mp ij} = 1.$$

Tensor perturbations in terms of these circularly polarized basis vectors are given by,

$$h_{ij}(\vec{k},\eta) = h^+(\vec{k},\eta)e^+_{ij} + h^-(\vec{k},\eta)e^-_{ij}. \tag{5}$$

The GW amplitude in these two polarization modes can be represented by $h^{\aleph}$ where $\aleph = +, -$ or $\aleph = +, \times$ depending on whether it is linearly or circularly polarized. The

GW equation for the amplitude in appropriate basis becomes

$$h''_{\aleph} + \frac{2a'}{a} h'_{\aleph} + k^2 h_{\aleph} = 8\pi G a^2 (\rho + p)\Pi_{\aleph}. \tag{6}$$

where $\Pi_{\aleph}$ is defined as $\Pi_{\aleph} \equiv [1/(\rho + p)]\bar{T}^{TT}_{\aleph}$.

A. The GW energy spectrum

In the next section, we will see that for statistically homogeneous and isotropic EM fields, $\langle \Pi_{ij}(\vec{k},\eta)\Pi^{ij}(\vec{k'},\eta)\rangle$ is proportional to $\delta(\vec{k}-\vec{k'})$ and some function of k and η. Using this fact, the above relation implies that tensor perturbation h_{ij} also satisfies the following property,

$$\langle h'_{ij}(\vec{k},\eta)h'^{ij}(\vec{k'},\eta)\rangle \propto \delta(\vec{k}-\vec{k'}) \times F(k,\eta) \tag{7}$$

for some function $F(k,\eta)$. From this property and using the expansions given in Eq. (4) and in Eq. (5), we express $\langle h'_{ij}(\vec{k},\eta)h'^{ij*}(\vec{k'},\eta)\rangle$ as,

$$\langle h'_{ij}(\vec{k},\eta)h'^{ij*}(\vec{k'},\eta)\rangle = (2\pi)^3\delta(\vec{k}-\vec{k'})\left(\left|\frac{dh^T(k,\eta)}{d\eta}\right|^2 + \left|\frac{dh^\times(k,\eta)}{d\eta}\right|^2\right) = (2\pi)^3\delta(\vec{k}-\vec{k'})\left(\left|\frac{dh^+(k,\eta)}{d\eta}\right|^2 + \left|\frac{dh^-(k,\eta)}{d\eta}\right|^2\right). \tag{8}$$

After substituting Eq. (8) in Eq. (2), we get

$$\frac{d\rho_{\rm GW}}{d\ln k} = \frac{k^3}{4(2\pi)^3 G a^2}\sum_{\aleph}\left(\left|\frac{dh^{\aleph}(k,\eta)}{d\eta}\right|^2\right). \tag{9}$$

Further, after normalizing the gravitational energy density with background energy density at present (ρ_{c_0}), we get

$$\left.\frac{d\Omega_{\rm GW}}{d\ln k}\right|_0 = \left.\frac{d\Omega_{\rm GW}}{d\ln k}\right|_\eta a^4(\eta) = \frac{k^3 a^2}{4(2\pi)^3 G\rho_{c_0}}\sum_{\aleph}\left(\left|\frac{dh^{\aleph}(k,\eta)}{d\eta}\right|^2\right), \tag{10}$$

where, in the above expression we have, as before, defined as, $d\Omega_{\rm GW}/d\ln k = (1/\rho_{c_0})d\rho_{\rm GW}/d\ln k$.

Our analysis involves an early matter dominated era between the end of inflation and before reheating followed by radiation dominated era post reheating. In Secs. II B and II C, we solve the GW evolution equation in these eras. We consider the following evolution of scale factor during these era,

$$a = \begin{cases} \frac{a_{eq}^2 H_{eq}}{4\eta_R}(\eta+\eta_R)^2, & \eta_e \le \eta \le \eta_R \\ a_{eq}^2 H_{eq}\eta, & \eta \ge \eta_R. \end{cases} \tag{11}$$

Here η_e and η_R are the conformal time at the end of inflation and the epoch of reheating, respectively. The scale factor and Hubble parameter at the epoch of radiation-matter equality are denoted, respectively by, a_{eq} and H_{eq}. The above form of the scale factor evolution in Eq. (11) ensures the continuity of a and H across η_R. We need to solve for the evolution of the h_{ij} sourced by the EM fields generated in the pre-reheating stage ($\eta \le \eta_R$) and the post reheating stage ($\eta \ge \eta_R$).

B. Evolution of h_{ij} for $\eta \le \eta_R$

During the epoch $\eta_e \le \eta \le \eta_R$, we define dimensionless variable $w \equiv k(\eta+\eta_R)$ and use the relation (11). In terms of this variables, Eq. (6) reduces to,

$$\frac{d^2h^{\aleph}}{dw^2} + \frac{4}{w}\frac{dh^{\aleph}}{dw} + h^{\aleph} = \frac{12}{w^2}\Pi^{\aleph}. \tag{12}$$

The homogeneous solutions of this equation are $(j_1(w)/w)$ and $(y_1(w)/w)$ (Here $j_1(w)$ and $y_1(w)$ are first order spherical Bessel functions of first and second kind, respectively). The complete solution of this equation is,

$$h^{\aleph}(\vec{k},w) = c_1\frac{j_1(w)}{w} + c_2\frac{y_1(w)}{w} + \frac{-j_1(w)}{w}\int_{w_i}^{w} dw_1 (12\Pi^{\aleph}(\vec{k},w_1))w_1^2\frac{y_1(w_1)}{w_1} + \frac{y_1(w)}{w}\int_{w_i}^{w} dw_1 (12\Pi^{\aleph}(\vec{k},w_1))w_1^2\frac{j_1(w_1)}{w_1} \tag{13}$$

Here c_1 and c_2 are constants which are determined by the matching of $h^{\aleph}$ and its derivative at the epoch just before and just after the end of inflation. In our model of inflationary magnetogenesis, the spectral magnetic field energy density is proportional to the fourth power of the Hubble parameter for a scale invariant magnetic field spectrum during inflation. Since the energy scale of inflation in our model is very low, the energy density of the magnetic field as well as the gravitational waves generated in the process is small during inflation. The corresponding contribution to the homogeneous part of the above solution is small compared to the contribution from

the source term. Therefore in the above solution, the main contribution to the GW energy density come from the terms with the source, which itself is generated during $\eta_e \leq \eta \leq \eta_R$.

C. Evolution of h_{ij} for $\eta \geq \eta_R$

In the radiation dominated era, in terms of the dimensionless variable $x \equiv k\eta$, Eq. (6) reduces to,

$$\frac{d^2h^{\aleph}}{dx^2}+\frac{2}{x}\frac{dh^{\aleph}}{dx}+h^{\aleph}=\frac{4}{x^2}\Pi^{\aleph}. \tag{14}$$

The homogeneous solution of this equation are zeroth order spherical Bessel function $j_0(x) = \sin(x)/x$ and $y_0(x) = -\cos(x)/x$. The complete solution of this equation is,

$$h^{\aleph}(\vec{k},x) = d_1 j_0(x) + d_2 y_0(x) - 4j_0(x)\int_{x_R}^{x} dx_1 \Pi^{\aleph}(\vec{k},x_1)y_0(x_1) + 4y_0(x)\int_{x_R}^{x} dx_1 \Pi^{\aleph}(\vec{k},x_1)j_0(x_1). \tag{15}$$

In the above expression, x_R is the value of variable x at reheating ($\eta = \eta_R$), while d_1 and d_2 are constants which are determined by matching h_{ij} and its derivative at $\eta = \eta_R$. Since we will be calculating the GWs spectrum due to the nonhelical as well as helical EM field, we first estimate the energy momentum tensor for such field.

III. ENERGY MOMENTUM TENSOR OF THE SOURCE

To calculate the GW energy spectrum we need to calculate the anisotropic stress tensor of the source. The energy momentum tensor of the electromagnetic field is given by,

$$T_{\mu\nu} = \frac{1}{4\pi}\left(g^{\alpha\beta}F_{\mu\alpha}F_{\nu\beta} - \frac{g_{\mu\nu}}{4}F^{\alpha\beta}F_{\alpha\beta}\right).$$

Anisotropic stress tensor is given by the transverse traceless projection of the spatial part of the energy momentum tensor. Spatial part of the energy momentum tensor is,

$$T_{ij}(\vec{x},\eta) = \frac{1}{4\pi}\left(B_i(\vec{x},\eta)B_j(\vec{x},\eta) + E_i(\vec{x},\eta)E_j(\vec{x},\eta) - \frac{1}{2}g_{ij}B^mB_m - \frac{1}{2}g_{ij}E^mE_m\right) \tag{16}$$

where

$$E_i = \frac{1}{a}F_{i0} = -\frac{1}{a}A_i' \quad \text{and} \quad B_i = \frac{1}{2a}\epsilon^*_{ijk}\delta^{jl}\delta^{km}F_{lm} = \frac{1}{a}\epsilon^*_{ijk}\delta^{jl}\delta^{km}\partial_l A_m$$

are the covariant components of the electric and magnetic field with respect to the comoving observer with four velocity $u^\mu \equiv (1/a, 0, 0, 0)$ [83]. Here A_i the is spatial part of the EM 4-potential and ϵ^*_{ijk} is 3-d fully antisymmetric symbol with $\epsilon^*_{123} = 1$. We are interested in the evolution of $\langle T^{TT}_{ij}(\vec{k},\eta)\bar{T}^{*ij}(\vec{k'},\eta')\rangle$ to calculate $\rho_{\rm GW}$. This is given by

$$\langle \bar{T}_{ij}(\vec{k},\eta)\bar{T}^{*kl}(\vec{k'},\eta')\rangle = \left(\frac{1}{4\pi a^4(\eta)}\right)\left(\frac{1}{4\pi a^4(\eta')}\right)\left(\int\frac{d^3q}{(2\pi)^3}\int\frac{d^3q'}{(2\pi)^3}P^{mn}_{ij}P^{kl}_{ab}(\langle\tilde{B}_m(\vec{q},\eta)\tilde{B}^*_n(\vec{q}-\vec{k},\eta) \times \tilde{B}^{*a}(\vec{q'},\eta')\tilde{B}^b(\vec{q'}-\vec{k'},\eta')\rangle + \langle\tilde{E}_m(\vec{q},\eta)\tilde{E}^*_n(\vec{q}-\vec{k},\eta)\tilde{E}^{*a}(\vec{q'},\eta')\tilde{E}^b(\vec{q'}-\vec{k'},\eta')\rangle)\right). \tag{17}$$

Here $P^{mn}_{ij} = P^m_i P^n_j - 1/2P_{ij}P^{mn}$ and tilde over the quantities represents their comoving values ($\tilde{B}_b(\vec{q},\eta) \equiv B_b(\vec{q},\eta)/a(\eta)$ and $\tilde{B}^b(\vec{q},\eta) \equiv B^b(\vec{q},\eta)/a^3(\eta)$). We have neglected the contribution of the cross terms of electric and magnetic field because those terms are always subdominant for our case of interest. From Eq. (17) it is clear that calculations of $\langle \bar{T}_{ij}(\vec{k},\eta)\bar{T}^{*kl}(\vec{k'},\eta')\rangle$ involves $(\langle\tilde{B}_m(\vec{q},\eta)\tilde{B}^*_n(\vec{q}-\vec{k},\eta)\tilde{B}^{*a}(\vec{r},\eta')\tilde{B}^b(\vec{r}-\vec{k'},\eta')\rangle$. Since the nature of the magnetic field generated in our model is Gaussian, we can express these four point correlation functions in terms of the two point correlation functions.

$$\langle \tilde{B}_m(\vec{q},\eta)\tilde{B}^*_n(\vec{q}-\vec{k},\eta)\tilde{B}^{*a}(\vec{r},\eta')\tilde{B}^b(\vec{r}-\vec{k}',\eta')\rangle = \langle \tilde{B}_m(\vec{q},\eta)\tilde{B}^*_n(\vec{q}-\vec{k},\eta)\rangle\langle \tilde{B}^{*a}(\vec{r},\eta')\tilde{B}^b(\vec{r}-\vec{k}',\eta')\rangle + \langle \tilde{B}_m(\vec{q},\eta)\tilde{B}^{*a}(\vec{r},\eta')\rangle\langle \tilde{B}^*_n(\vec{q}-\vec{k},\eta)\tilde{B}^b(\vec{r}-\vec{k}',\eta')\rangle + \langle \tilde{B}_m(\vec{q},\eta)\tilde{B}^b(\vec{r}-\vec{k}',\eta')\rangle\langle \tilde{B}^*_n(\vec{q}-\vec{k},\eta)\tilde{B}^{*a}(\vec{r},\eta')\rangle \quad (18)$$

In Eq. (18), we require unequal time correlation of the magnetic fields. For this we followed the analysis in [20,84] and represent the unequal time correlation of the source in terms of the product of the equal time correlation, $\langle \tilde{B}_i(\vec{k},\eta)\tilde{B}_j(\vec{k}',\eta)\rangle$ and a two time correlation function $C_B(k,\eta,\eta')$, which depends on these different times as follows,

$$\langle \tilde{B}_i(\vec{k},\eta)\tilde{B}_j(\vec{k}',\eta')\rangle = \langle \tilde{B}_i(\vec{k},\eta)\tilde{B}_j(\vec{k}',\eta)\rangle C_B(k,\eta,\eta'). \quad (19)$$

It is evident from the above relation that for equal time correlation $C_B(k,\eta,\eta)=1$. To proceed further, we need to know the equal time correlation function of the electric and magnetic field. We divide the further study in two parts depending upon the nature of the generated EM field; nonhelical and helical nature. Similar analysis has also been done in a previous study [82]. For the sake of completeness, we reproduce those results further in this section. The only difference in our analysis with respect to the previous studies is that we have explicitly written the unequal time correlation part in the final expressions.

A. Nonhelical EM fields

For nonhelical magnetic and electric fields, we represent the two point correlation function in terms of the power spectrum as follows [22],

$$\langle \tilde{B}_i(k,\eta)\tilde{B}^*_j(k',\eta)\rangle = (2\pi)^3\delta(\vec{k}-\vec{k}')(\delta_{ij}-\hat{k}_i\hat{k}_j)P_{SB}(k,\eta)$$
$$\langle \tilde{E}_i(k,\eta)\tilde{E}^*_j(k',\eta)\rangle = (2\pi)^3\delta(\vec{k}-\vec{k}')(\delta_{ij}-\hat{k}_i\hat{k}_j)P_{SE}(k,\eta). \quad (20)$$

In the above expression, we have assumed that the distribution of the generated electric and magnetic field is homogeneous and isotropic. The delta function, $\delta(\vec{k}-\vec{k}')$ in the above expression and the dependence of power spectrum P_{SB} only on the magnitude of the $\vec{k}$ arise because of the this homogeneous and isotropic nature of the electromagnetic field distribution. The projection tensor $(\delta_{ij}-\hat{k}_i\hat{k}_j)$ in the above expression ensures the divergence less nature of the magnetic field. We also have this projection tensor in the electric field correlation function as during the EM field generation, charge particles density is negligible. Hence, the electric field can be assumed to have zero divergence.

Equations (17), (18), (19), and (20) imply

$$\langle \bar{T}_{ij}(\vec{k},\eta)\bar{T}^{*ij}(\vec{k}',\eta')\rangle = \frac{1}{a^4(\eta)a^4(\eta')}(f_B(k,\eta,\eta')+f_E(k,\eta,\eta'))(2\pi)^3\delta(\vec{k}-\vec{k}'). \quad (21)$$

Here,

$$f_{B,E}(k,\eta,\eta') = \frac{1}{4(2\pi)^5}\int d^3q[P_{SB,SE}(q,\eta)P_{SB,SE}(|\vec{k}-\vec{q}|,\eta)(1+\gamma^2+\beta^2+\gamma^2\beta^2)]C_{B,E}(q,\eta,\eta')C_{B,E}(|\vec{k}-\vec{q}|,\eta,\eta'). \quad (22)$$

In the above expression $\gamma = \hat{k}\cdot\hat{q}$ and $\beta = \widehat{k}\cdot\widehat{k-q}$.

To get the individual mode contribution, we express $\bar{T}_{ij}(\vec{k},\eta)$ in terms of the linear polarization basis.

$$\bar{T}_{ij}(\vec{k},\eta) = \bar{T}^T(\vec{k},\eta)e^T_{ij} + \bar{T}^\times(\vec{k},\eta)e^\times_{ij}$$

Using this we get,

$$\langle \bar{T}_{ij}(\vec{k},\eta)\bar{T}^{*ij}(\vec{k}',\eta')\rangle = (|\bar{T}^T|^2(k,\eta,\eta')+|\bar{T}^\times|^2(k,\eta,\eta'))(2\pi)^3\delta(\vec{k}-\vec{k}'). \quad (23)$$

In this case, the source is such that the contribution to both the modes (T and $\times$) are equal. From Eq. (21) and Eq. (23), we get,

$$|\bar{T}^T|^2(k,\eta,\eta') = |\bar{T}^\times|^2(k,\eta,\eta') = \frac{1}{2}\frac{1}{a^4(\eta)a^4(\eta')}(f_B(k,\eta,\eta')+f_E(k,\eta,\eta')).$$

B. Helical EM fields

We follow a similar procedure for the case of helical field. The only difference that will arise is that there is an additional antisymmetric contribution to the 2-point correlation function. For helical EM field, we have Caprini *et al.* [82],

$$\langle \tilde{B}_i(k,\eta)\tilde{B}_j^*(k',\eta)\rangle = (2\pi)^3\delta(\vec{k}-\vec{k'})((\delta_{ij}-\hat{k}_i\hat{k}_j)P_{SB}(k,\eta)+i\epsilon_{ijm}\hat{k}_m P_{AB}(k,\eta))$$
$$\langle \tilde{E}_i(k,\eta)\tilde{E}_j^*(k',\eta)\rangle = (2\pi)^3\delta(\vec{k}-\vec{k'})((\delta_{ij}-\hat{k}_i\hat{k}_j)P_{SE}(k,\eta)+i\epsilon_{ijm}\hat{k}_m P_{AE}(k,\eta)) \quad (24)$$

The term containing P_{AB}, P_{AE} are the antisymmetric parts of two point correlation tensor. Equations (24), (18), and (17) imply

$$\langle \bar{T}_{ij}(\vec{k},\eta)\bar{T}^{*ij}(\vec{k'},\eta')\rangle = \frac{1}{a^4(\eta)a^4(\eta')}(g_B(k,\eta,\eta')+g_E(k,\eta,\eta'))(2\pi)^3\delta(\vec{k}-\vec{k'}), \quad (25)$$

where,

$$g_{B,E}(k,\eta,\eta') = \frac{1}{4(2\pi)^5}\int d^3q[P_{SB,SE}(q,\eta)P_{SB,SE}(|\vec{k}-\vec{q}|,\eta)(1+\gamma^2+\beta^2+\gamma^2\beta^2) + 4\gamma\beta P_{AB,AE}(q,\eta)P_{AB,AE}(|\vec{k}-\vec{q}|,\eta)]C_{B,E}(q,\eta,\eta')C_{B,E}(|\vec{k}-\vec{q}|,\eta,\eta'). \quad (26)$$

Here $\gamma = \hat{k}\cdot\hat{q}$ and $\beta = \hat{k}\cdot\widehat{k-q}$.

To write down the individual mode contribution for this case, we express $\Pi_{ij}(\vec{k})$ in terms of the circular polarization basis.

$$\bar{T}_{ij}(\vec{k},\eta) = \bar{T}^{+}(k,\eta)e_{ij}^{+} + \bar{T}^{-}(k,\eta)e_{ij}^{-}$$
$$\langle \bar{T}_{ij}(\vec{k},\eta)\bar{T}^{*ij}(\vec{k'},\eta')\rangle = (|\bar{T}^{+}|^2(k,\eta,\eta')+|\bar{T}^{-}|^2(k,\eta,\eta'))(2\pi)^3\delta(\vec{k}-\vec{k'})$$

In this case, the individual mode $(+,-)$ not only involves the terms arising from the terms containing $P_S P_S$ and $P_A P_A$ but also the cross term containing $P_S P_A$. These terms contribute to individual mode as follows,

$$|\bar{T}^{-}|^2(k,\eta,\eta') = \frac{1}{2}\frac{1}{a^4(\eta)a^4(\eta')}(g_B(k,\eta,\eta')+g_E(k,\eta,\eta')+h_B(k,\eta,\eta')+h_E(k,\eta,\eta'))$$
$$\text{and}\quad \bar{T}^{+}|^2(k,\eta,\eta') = \frac{1}{2}\frac{1}{a^4(\eta)a^4(\eta')}(g_B(k,\eta,\eta')+g_E(k,\eta,\eta')-h_B(k,\eta,\eta')-h_E(k,\eta,\eta')).$$

Here

$$h_{B,E}(k,\eta,\eta') = \frac{1}{4(2\pi)^5}\int d^3q[P_{SB,SE}(q,\eta)P_{AB,AE}(|\vec{k}-\vec{q}|,\eta)4(1+\gamma^2)\beta]C_{B,E}(q,\eta,\eta')C_{B,E}(|\vec{k}-\vec{q}|,\eta,\eta')$$

IV. GRAVITATIONAL WAVE SPECTRUM EXPECTED IN OUR MODEL

In our model, to address the strong coupling and back-reaction problems of inflationary magnetogenesis, we have taken a particular evolution of the coupling function, f which evolves with time both during as well as in the era after inflation till reheating. This function increases during inflation and transits to a decaying phase post inflation. We have assumed that the era between the end of inflation and the beginning of reheating is matter dominated. After this matter dominated era, reheating takes place and standard radiation dominance starts. During inflation the magnetic field spectrum is scale invariant but the strength is very low compared to the background energy density because of the low scale of inflation. In the post inflation era when coupling function, f decreases, the scale invariant contribution to the magnetic spectrum decreases but contribution from the next order gets amplified on the superhorizon scales. This postinflationary era ends when the EM energy density is ϵ times the background energy density and after this reheating takes place and EM energy density evolves like radiation. The magnetic field spectrum generated in our model is a blue spectrum, $d\tilde{\rho}_B(k,\eta)/d\ln k \propto k^4$, where $\tilde{\rho}_B$ is the comoving magnetic energy density.

The main contribution to the GW energy spectrum takes place during the end phase of the postinflationary matter dominated era. During this era both electric and magnetic fields contribute to the production of GW. However after reheating, electric fields get shorted out because of the large conductivity of the universe and only magnetic field contributes to the production of GW. We have considered scenarios of magnetogenesis where nonhelical fields are generated [80] as well as a scenario [81] where the EM field generated is almost fully helical. In subsequent sections, we therefore consider GW energy spectrum generated due to both nonhelical and helical EM fields.

Using Eq. (10), GW energy spectrum can be expressed as,

$$\left.\frac{d\Omega_{\rm GW}}{d\ln k}\right|_0 = \frac{k^3a^2}{4(2\pi)^3G\rho_c}\sum_{\aleph}\left(\left|\frac{dh^{\aleph}(\eta)}{d\eta}\right|^2\right) = \frac{\Omega_R k^3x^2}{12\pi^2}\sum_{\aleph}\left(\left|\frac{dh^{\aleph}(x)}{dx}\right|^2\right), \tag{27}$$

where we can calculate $|dh^{\aleph}(x)/dx|^2$ using Eq. (15). In the limit $x \gg 1$, we get

$$\left|\frac{dh^{\aleph}(k,x)}{dx}\right|^2 = \frac{1}{2x^2}(|d_1|^2+|d_2|^2) + \frac{8}{x^2}\int_{x_R}^{x_{\nu d}}\int_{x_R}^{x_{\nu d}}\frac{dx_1dx_2}{x_1x_2}\cos(x_2-x_1)|\Pi^{\aleph}|^2(k,x_1,x_2). \tag{28}$$

The calculation of the above expression is given in Appendix A. The expression for $|\Pi^{\aleph}|^2$ is as given in Eq. (29). In the above expression, for the second term the limits of the integration are from the epoch of reheating to the neutrino decoupling epoch ($x_{\nu d} = k\eta_{\nu d}$) and only magnetic field contributes for this case as electric field gets shorted out by the large conductivity of the universe after reheating. After neutrino decoupling epoch, anisotropic stress of the magnetic field is balanced by the anisotropic stress of the neutrinos [85] and there is no further production of GW take place. The expressions for $|d_1|^2$ and $|d_2|^2$ contains the $|\Pi^{\aleph}|^2(k,\eta,\eta')$ and also the different time correlation function $C_{B,E}(k,\eta,\eta')$. To evaluate $|\Pi^{\aleph}|^2(k,\eta,\eta')$, we need to know two point correlation of electric and magnetic fields which takes different forms for nonhelical and helical EM field as discussed in the Sec. III. Therefore, we perform further analysis in two parts depending upon the nonhelical and helical nature of the EM field.

A. Gravitational waves energy spectrum for nonhelical magnetic field

To evaluate the GW energy spectrum, we need to evaluate $|\Pi^{\aleph}|^2(k,\eta,\eta')$. Using $\Pi_{ij} = 1/(\rho+p)T^{TT}_{ij}$, we express $|\Pi^{\aleph}|^2$ in terms of $|\bar{T}^{\aleph}|^2$ which we have calculated in the Sec. III and we get,

$$|\Pi^{\aleph}|^2(k,\eta,\eta') = \frac{1}{(\rho+p)(\eta)}\frac{1}{(\rho+p)(\eta')}|\bar{T}^{\aleph}|^2(k,\eta,\eta'). \tag{29}$$

In the matter dominated era before reheating, $(\rho+p) \propto a^{-3}$, whereas, in the radiation dominated era post reheating, we have, $(\rho+p) \propto a^{-4}$. Using this, the above relation reduces to the following expression for nonhelical field,

$$|\Pi^{\aleph}|^2(k,\eta,\eta') = \begin{cases} \frac{a_R}{a(\eta)}\frac{a_R}{a(\eta')}\left(\frac{1}{\tilde{\rho}+\tilde{p}}\right)^2\frac{1}{2}(f_B(k,\eta,\eta')+f_E(k,\eta,\eta')), & \eta,\eta' \le \eta_R \\ \left(\frac{1}{\tilde{\rho}+\tilde{p}}\right)^2\frac{f_B(k,\eta,\eta')}{2}, & \eta,\eta' \ge \eta_R \end{cases} \tag{30}$$

In the above expression tilde over quantities represents their comoving values. As is evident from Eq. (22), to calculate f_B and f_E, we need to know the electric and magnetic field power spectrum in the matter dominated era after inflation and their evolution after reheating. These power spectra can be expressed in the form of spectral energy density of magnetic and electric fields as follows,

$$P_{SB,SE}(k,\eta) = \frac{(2\pi)^3}{k^3}\frac{d\tilde{\rho}_{B,E}(k,\eta)}{d\ln k}. \tag{31}$$

During the matter dominated era the electric and magnetic spectral energy density increase at a rate decided by how the coupling function decreases. In our model discussed in Sharma *et al.* [80], the coupling function $f \propto a^{-\beta}$

($\beta = 2N/N_r$ where N and N_r are the number of e-folds during inflation and after the end of inflation to reheating, respectively) and the comoving spectral electric and magnetic field energy density evolve as,

$$\frac{d\tilde{\rho}_B(k,\eta)}{d\ln k} = \begin{cases} D_1\left(\frac{k}{k_p(\eta)}\right)^4\left(\frac{\eta+\eta_R}{2\eta_R}\right)^{8\beta+2}, & k \le k_p(\eta), \quad \eta \le \eta_R \\ D_1\left(\frac{k}{k_p(\eta)}\right)^4\left(\frac{\eta_k+\eta_R}{2\eta_R}\right)^{8\beta+2}, & k \ge k_p(\eta), \quad \eta \le \eta_R \end{cases} \tag{32}$$

$$\frac{d\tilde{\rho}_E(k,\eta)}{d\ln k} = \begin{cases} D_2\left(\frac{k}{k_p(\eta)}\right)^2\left(\frac{\eta+\eta_R}{2\eta_R}\right)^{8\beta}, & k \le k_p(\eta), \quad \eta \le \eta_R \\ D_2\left(\frac{k}{k_p(\eta)}\right)^2\left(\frac{\eta_k+\eta_R}{2\eta_R}\right)^{8\beta}, & k \ge k_p(\eta), \quad \eta \le \eta_R \end{cases} \tag{33}$$

Here $k_p(\eta)$ is the mode where electric and magnetic spectral energy density peak. For the model discussed in [80], $k_p(\eta) = \beta k_H(\eta)$[1] where $k_H(\eta)$ is the mode corresponding to the horizon size at conformal time η. η_R is the epoch of reheating, and, D_1 and D_2 are, respectively, the amplitudes of spectral magnetic and electric energy densities at $k_0 = k_p(\eta_R)$ which is the comoving horizon scale at the epoch of reheating, denoted by the conformal time, $\eta = \eta_R$. Values of D_1 and D_2 depend on the fraction of electromagnetic energy density to background energy density at reheating and D_2 is 4 times the value of D_1 in our model of inflationary magnetogenesis. The above expression for the case $k \le k_p$ has been derived in the Ref. [80]. For the modes which enter during the matter dominated era ($k \ge k_0$), we approximate their spectral energy density by the value at $\eta = \eta_k$ when the mode enters the horizon. The contribution of these modes will not make much difference to the GW spectrum.

For this case, we know the exact time evolution of the EM field during the matter dominance era (see Ref. [80] for details). Thus we express the two point correlation function at different times in terms of the power spectrum of the electromagnetic fields with the help of the following correlation function,

$$C_B(k,\eta,\eta') = \left(\frac{\eta'+\eta_R}{\eta+\eta_R}\right)^{4\beta+1}$$

$$\text{and} \quad C_E(k,\eta,\eta') = \left(\frac{\eta'+\eta_R}{\eta+\eta_R}\right)^{4\beta} \quad \text{for } \eta, \quad \eta' < \eta_R.$$

After reheating, electric field does not contributes to GW spectrum as it gets shorted out due to the large conductivity of the universe. The spectrum of the magnetic field energy density at reheating is a blue spectrum which peaks at $k = k_0$ at reheating. After reheating the universe enters to the radiation dominated era from the matter dominated era. Larger and larger scale superhorizon modes begin to enter the horizon. Nonlinear processing of the magnetic field energy density becomes important when the Alfven crossing time becomes equal to the Hubble time i.e., $kV_A(k) = aH$ [87,88]. Here $V_A = \sqrt{(d\tilde{\rho}_B(k)/d\ln k)/(\tilde{\rho}+\tilde{p})}$ is the Alfven velocity for the mode k. For simplicity, we assume that nonlinear processing starts just after reheating. After the onset of nonlinear evolution of the magnetic field, the detailed analysis of their evolution requires numerical simulation [89–91]. Further, the calculation of the GW spectrum also requires numerical simulation which has been recently done in Ref. [92] for the magnetohydrodynamic turbulance in the early universe. Here we use the analytical results for the evolution of magnetic field energy density discussed in [87,88],

$$\frac{d\tilde{\rho}_B(k,\eta)}{d\ln k} = \begin{cases} D_1\left(\frac{k}{k_{NL}(\eta)}\right)^4\left(\frac{\eta}{\eta_R}\right)^{-\frac{4}{3}}, & k \le k_{NL}(\eta) \\ D_1\left(\frac{k}{k_{NL}(\eta)}\right)^{-\frac{2}{3}}\left(\frac{\eta}{\eta_R}\right)^{-\frac{4}{3}}, & k_\nu \ge k \ge k_{NL}(\eta) \end{cases} \tag{34}$$

where,

$$k_{NL}(\eta) = k_0\left(\frac{\eta}{\eta_R}\right)^{-\frac{1}{3}}. \tag{35}$$

Here k_ν is the wave number above which viscosity dominate and the spectrum becomes exponentially damped. We will refer to the branch of the magnetic spectrum, which develops due to the MHD turbulent cascade of energy to smaller and smaller scales, and with $d\tilde{\rho}_B/d\ln k \propto k^{-2/3}$ as the Kolmogorov branch. For the estimation of GW energy spectrum, we also need to know the unequal time correlation function of the magnetic field energy densities. To find the unequal time correlation requires numerical simulation. It has been approximated in Ref. [84] by the following expression, which we adopt,

$$C_B(k,\eta_1,\eta_2) = \begin{cases} \exp\left[\frac{-(\eta_1-\eta_2)^2}{2\tau_E^2(k,\eta_{\max})}\right], & k_\nu \ge k \ge k_{NL}(\eta_{\max}) \\ 1, & k \le k_{NL}(\eta_{\max}). \end{cases} \tag{36}$$

[1]In Refs. [81,86], we have taken $\beta \approx 1$ for the wave number where the magnetic and electric spectrum peak. However, for the calculation of the GW spectrum, we have taken the actual value of β.

Here $\eta_{\rm max} = Max[\eta_1, \eta_2]$ and

$$\tau_E(k,\eta) = \frac{1}{k\sqrt{\frac{1}{(\tilde{\rho}+\tilde{p})}\left\langle\frac{d\tilde{\rho}_B(k)}{d\ln k}\right\rangle}} \tag{37}$$

is the eddy turnover time for the mode k, assuming that these eddies have developed a velocity comparable to the Alfvén velocity. In the above expression

$$\left\langle\frac{d\tilde{\rho}_B(k)}{d\ln k}\right\rangle = \int_0^\infty d\ln k \frac{d\tilde{\rho}_B(k)}{d\ln k}.$$

After substituting the expression of $d\tilde{\rho}_B(k)/d\ln k$ from Eq. (34) in Eq. (37), we get

$$\tau_E^2(k,\eta) \approx \frac{2}{3k^2}\frac{\tilde{\rho}+\tilde{p}}{D_1}\left(\frac{\eta}{\eta_R}\right)^{4/3}. \tag{38}$$

Using the information of EM energy densities and correlation function in Eq. (36) applicable to this case, we evaluate the expression given in Eq. (28). To calculate GW energy spectra, we need to solve the integrals in Eq. (28) and substitute its value in Eq. (27). The exact estimation of these integrals cannot be done analytically and we will present numerical calculations below. However, one can get analytical estimate for the modes with $k < k_H$, which we can compare with corresponding numerical results. Before this, and to compare partially with the numerical results, we now consider an analytical estimate.

1. Analytical estimates

For $k < k_H$ the expression for $d\Omega_{\rm GW}/d\ln k|_0$ is given by,

$$\left.\frac{d\Omega_{\rm GW}}{d\ln k}\right|_0 = \frac{7\Omega_R}{5}\left(\frac{k}{k_0}\right)^3\left(\frac{D_2}{\tilde{\rho}+\tilde{p}}\right)^2\left(\frac{64\beta^2}{(1-4\beta)^2(8\beta+1)^2}\right) + c\Omega_R\left(\frac{D_1}{\tilde{\rho}+\tilde{p}}\right)^2\left(\frac{k}{k_0}\right)^3. \tag{39}$$

where,

$$k_0 = 1.72\times10^9\beta\left(\frac{g_R}{106.75}\right)^{1/6}\frac{T_R}{100\ \text{GeV}}\ \text{Mpc}^{-1} \tag{40}$$

and the corresponding frequency

$$\nu_0 = \frac{k_0}{2\pi} = 2.7\times10^{-6}\beta\left(\frac{g_R}{106.75}\right)^{1/6}\frac{T_R}{100\ \text{GeV}}\ \text{Hz} \tag{41}$$

[See Appendix B for details]. Here g_R is the relativistic degree of freedom at the epoch of reheating. In the above expression, the first part represents the analytical estimate of the contribution from EM field anisotropic stresses before reheating and the second part represents that from the magnetic field anisotropic stresses after reheating. This is compared with the results from numerical integration for the low wave numbers. Although the approximation used in deriving analytical estimate fails for $\nu > \nu_H$, we extrapolate the analytical estimates until the modes $\nu < \nu_0$ and show the comparison with the numerical result in Fig. 1. An estimate of the GW background amplitude can be obtained using (39) for the mode $k = k_0$. Adopting $T_R = 100$ GeV, $\Omega_R = 9.24\times10^{-5}$, $c = 0.31$ and $\beta = 6.37$ (if the ratio of EM energy density to the background energy density (ϵ) is one at reheating) gives,

$$\left.\frac{d\Omega_{\rm GW}}{d\ln k}\right|_{0(k=k_H)} \approx 1.7\times10^{-8}$$
$$\text{and}\quad \left.\frac{d\Omega_{\rm GW}}{d\ln k}\right|_{0(k=k_0)} \approx 4.3\times10^{-6}. \tag{42}$$

This amplitude decreases roughly as $D_1^2 \propto \epsilon^2$, and so is approximately 10^{-4} times smaller for $\epsilon = 10^{-2}$. This is an approximate estimate as β also changes slowly with ϵ. Note

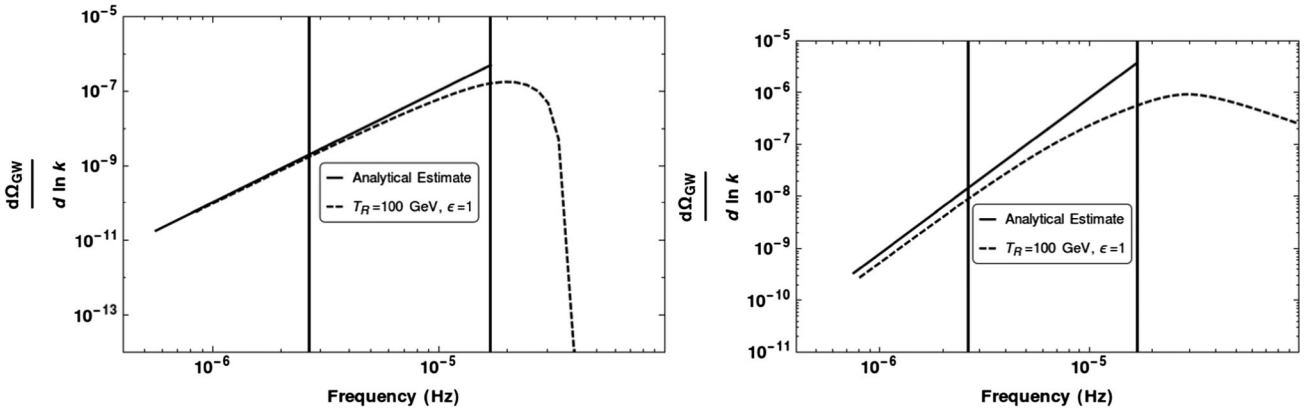

FIG. 1. In this figure we plot the GW energy spectrum obtained from the numerical calculation along with the analytical estimate given in Eq. (39). In the left panel, we show the analytical estimate for the electric field anisotropies contribution to the GW spectrum and in the right panel show the analytical estimate for the magnetic fields anisotropic stresses contribution after reheating. The first and second vertical gridlines correspond to the frequencies ν_H (frequency corresponding to wave number k_H) and ν_0 (frequency corresponding to wave number k_0) respectively. We plotted the analytical estimates for the modes $\nu \le \nu_0$. Although the approximation used in deriving analytical estimate fails for $\nu > \nu_H$, we extrapolate the analytical estimates until the modes $\nu < \nu_0$.

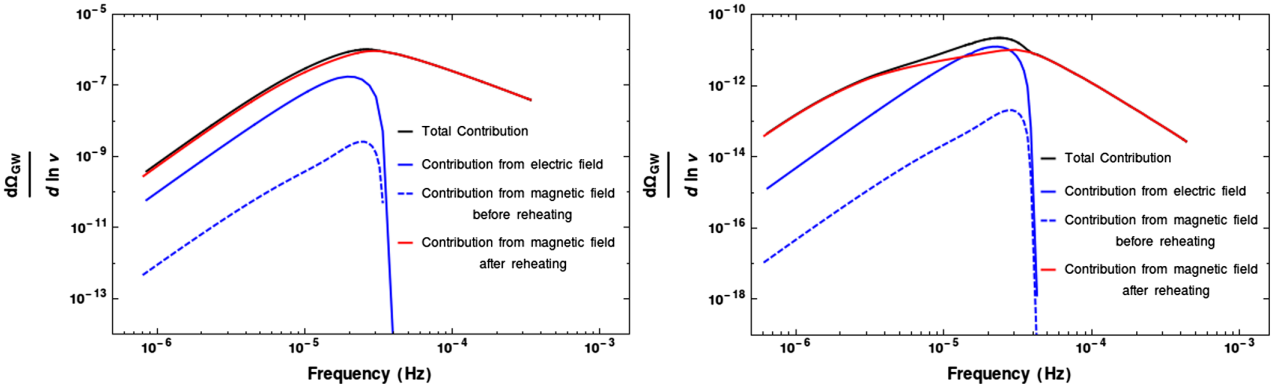

FIG. 2. In this figure we plot the different contribution to the GW energy spectrum generated from the EM field anisotropic stresses (nonhelical case). In the left and right panel, we assume $\epsilon = 1$ and $\epsilon = 10^{-2}$, respectively. The blue and the dashed blue lines, respectively, represent the contribution to the GW energy spectrum from electric and magnetic fields anisotropic stresses before reheating. The red curve represent the contribution from the magnetic field anisotropic stresses after reheating and the black curve represent the sum of all these contributions.

that our analytical estimate for the GW energy spectrum differs by a factor of 2 for $k = k_H$ and 5 for $k = k_0$ by the numerical estimate. Our primary aim to give the analytical estimate is to know the spectral nature which matches well with the numerical estimate within the region where the approximation made in analytical estimate is valid as shown in Fig. 1.

2. Numerical results for GW spectrum

We calculate the GW spectrum for different reheating temperatures T_R and different fractions (ϵ) of the EM field energy density to the background energy density at the time of reheating. Our model of magnetic field generation during inflation, requires reheating to be below an energy scale of 5000 GeV to satisfy the constraints from the γ-ray observations [80] which changes to the value 500 GeV in case of helical nature of EM field [81]. At the same time, it should be above 5 MeV to account for big bang nucleosynthesis [93]. We therefore give results for some representative values of T_R which lie in this range. Each wave number k is also be converted into the frequency ν of the GW using $\nu = kc/2\pi$.

In Fig. 2, we have shown the different contribution to the GW energy spectrum for $\epsilon = 1$ and $\epsilon = 10^{-2}$ assuming $T_R = 100$ GeV. The blue and dashed blue curve shown the contribution from the electric and magnetic fields spectrum before reheating, respectively. The red curve shows the contribution from the magnetic field spectrum after reheating. As is evident from this figure, the main contribution to the GW energy spectrum comes from the magnetic field anisotropic stresses after reheating for $\epsilon = 1$. However, for $\epsilon = 10^{-2}$, the contribution from electric field anisotropic stresses dominate around the peak of the total GW spectrum elsewhere it is dominated by the contribution from magnetic field anisotropic stresses after reheating. This leads to an extra bump type feature around the peak in the resultant GW energy spectrum for $\epsilon = 10^{-2}$.

In the upper panel of Fig. 3, we plot GW energy spectrum for the reheating scale $T_R = 100$ GeV and $T_R = 1000$ GeV and also for $\epsilon = 1$ and $\epsilon = 10^{-2}$. The peak of the GW spectrum lies approximately around the peak of the EM field spectrum at reheating. Note that the electric and magnetic field spectra peak at the frequency corresponding to a wave number which is β times of the horizon wave number at reheating and this $\propto 1/T_R$. This relation, however, is approximate since β also depends mildly on the value of T_R. Therefore the frequency at which GW spectrum has its peak, has a roughly linear behavior with the reheating temperature, T_R. It is also weakly dependent on ϵ corresponding to the same T_R due to change in the value of β for different ϵ. The peak value of the GW spectrum is $d\Omega_{\rm GW}/d\ln(k) \approx 9.6 \times 10^{-7}$ at the frequency 30 μHz for $T_R = 100$ GeV and 4.1×10^{-7} at the frequency 1 mHz for $T_R = 1000$ GeV assuming $\epsilon = 1$ for both the cases. For $\epsilon = 10^{-2}$, the peak value of the GW spectrum changes to 2.0×10^{-11} for $T_R = 100$ GeV and to 1.5×10^{-12} for $T_R = 1000$ GeV, respectively. The approximate dependence $\Omega_{\rm GW} \propto \epsilon^2$ for a given T_R is because the amplitude of tensor metric perturbations depend on the amplitude of the anisotropic stress of the EM field (which is $\propto \epsilon$) and $\Omega_{\rm GW}$ depends quadratically on these metric perturbations. For the modes $k \leq k_H$ (the mode where GW energy spectrum peaks), our analytical estimate in Eq. (39) suggests that the spectrum is proportional to k^3. As is evident from Fig. 2, for the modes $k > k_{\rm peak}$, the GW energy spectrum is proportional to $k^{-5/3}$ for $\epsilon = 1$ and $k^{-8/3}$ for $\epsilon = 10^{-2}$. The slope $k^{-8/3}$ for the case $\epsilon = 10^{-2}$ matches with the result obtained from the numerical simulation in Pol *et al.* [92]. The frequency at which the GW energy spectrum peaks, $\nu_{\rm peak} \approx 2\nu_0$ [ν_0 is the frequency corresponding to the wave number $k_0 = k_p(\eta_R)$] for any T_R and ϵ.

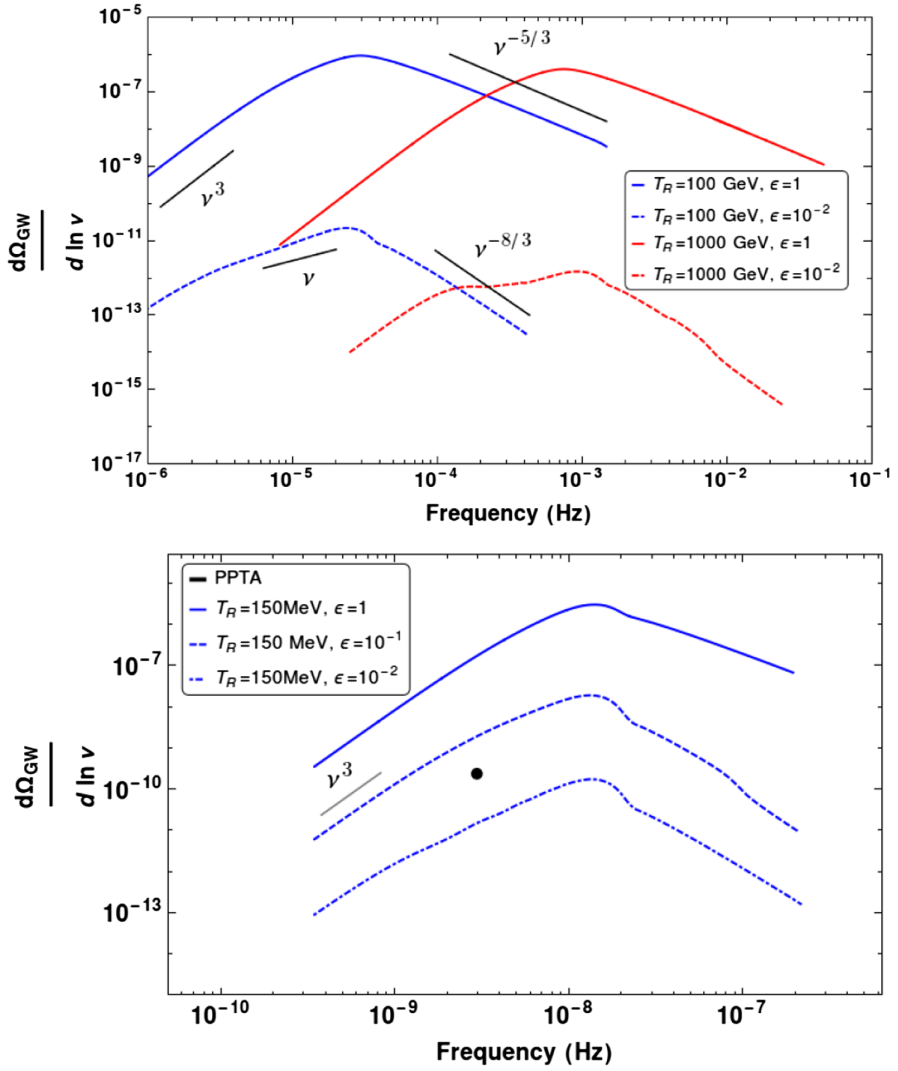

FIG. 3. In this figure we plot the GW energy spectrum generated from the EM field anisotropic stresses (nonhelical case). In the upper panel, we plot GW energy spectrum for the reheating scale $T_R = 100$ GeV and $T_R = 1000$ GeV and also for the different fraction (ϵ) of EM field energy density to the background energy density at reheating. In the lower panel, we plot the GW spectrum for the reheating scale at $T_R = 150$ MeV. The black dot point in the lower panel of the figure represent the limit on the GW energy spectrum at the nanohertz scale obtained from the Parkes pulsar timing array (PPTA) [94].

We show the predicted GW spectrum for the lower reheating scale at $T_R = 150$ MeV in the lower panel of Fig. 3. For the modes $k \leq k_{\rm peak}$, the spectrum is proportional to k^3 similar to other reheating scales. For this case, the GW spectrum has the peak value 3.1×10^{-6} at the frequency 1.6×10^{-8} Hz. Present limits on the GW spectrum at nanohertz frequencies are obtained from Parkes pulsar timing array (PPTA) [94]. This is shown as a black dot in the lower panel of the figure. Since PPTA does not detect any GW with this sensitivity, from Fig. 3 we conclude that for $T_R = 150$ MeV, $\epsilon < 10^{-1}$. This limit will become even stronger for those scenarios in which reheating is below 150 MeV and as the pulsar timing array limits improve in the future.

B. Gravitational waves energy spectrum for helical EM fields

If we generalize the Ratra model of inflationary magnetogenesis and add a parity breaking term $(f^2 F_{\mu\nu}\tilde{F}^{\mu\nu})$ to the Lagrangian density, the generated magnetic field is almost fully helical. Here $\tilde{F}^{\mu\nu}$ is the dual tensor of the EM tensor. In the standard electromagnetism with f constant, this term is a total divergence term and does not contribute to the evolution of the electromagnetic field. However when f is time dependent and conformal invariance of the EM theory is broken, this term contributes to the evolution of the EM field. It introduces a mixing between the two vector potential modes in the linear polarization basis. In terms of the helicity basis (or circular polarization basis),

left and right circular polarization modes decouple and satisfy different evolution equations. It turns out that the amplitude of one of the heilcal mode is larger than the other at the end of generation era and the net generated magnetic field is of helical nature. In our model [81], the generated magnetic field is almost fully helical. This results in the generated stochastic GW to be predominantly circularly polarized. The calculations of the GW background which is generated by such a field is on similar lines as for the nonhelical case. Hence, we only give the results of the GW, magnetic and electric energy spectrum.

For this case $|\Pi^{\aleph}|^2(k,\eta,\eta')$ is given by,

$$|\Pi^{-}|^2(k,\eta,\eta') = \begin{cases} \frac{a_R}{a(\eta)}\frac{a_R}{a(\eta')}\left(\frac{1}{\tilde{\rho}+\tilde{p}}\right)^2 \frac{1}{2}(g_B(k,\eta,\eta') + g_E(k,\eta,\eta') + h_B(k,\eta,\eta') + h_E(k,\eta,\eta')), & \eta,\eta' \le \eta_R \\ \left(\frac{1}{\tilde{\rho}+\tilde{p}}\right)^2 \frac{1}{2}(g_B(k,\eta,\eta') + h_B(k,\eta,\eta'), & \eta,\eta' \ge \eta_R \end{cases} \tag{43}$$

$$|\Pi^{+}|^2(k,\eta,\eta') = \begin{cases} \frac{a_R}{a(\eta)}\frac{a_R}{a(\eta')}\left(\frac{1}{\tilde{\rho}+\tilde{p}}\right)^2 \frac{1}{2}(g_B(k,\eta,\eta') + g_E(k,\eta,\eta') - h_B(k,\eta,\eta') - h_E(k,\eta,\eta')), & \eta,\eta' \le \eta_R \\ \left(\frac{1}{\tilde{\rho}+\tilde{p}}\right)^2 \frac{1}{2}(g_B(k,\eta,\eta') - h_B(k,\eta,\eta'), & \eta,\eta' \ge \eta_R \end{cases} \tag{44}$$

The above expressions imply that $|\Pi^{-}|^2$ is larger than $|\Pi^{+}|^2$ by an amount $h_B(k,\eta,\eta') + h_E(k,\eta,\eta')$. Adding Eq. (43) and Eq. (44), we get

$$|\Pi^{-}|^2(k,\eta,\eta') + |\Pi^{+}|^2(k,\eta,\eta') = \begin{cases} \frac{a_R}{a(\eta)}\frac{a_R}{a(\eta')}\left(\frac{1}{\tilde{\rho}+\tilde{p}}\right)^2 \frac{1}{2}(g_B(k,\eta,\eta') + g_E(k,\eta,\eta')), & \eta,\eta' \le \eta_R \\ \left(\frac{1}{\tilde{\rho}+\tilde{p}}\right)^2 \frac{1}{2}(g_B(k,\eta,\eta'), & \eta,\eta' \ge \eta_R \end{cases} \tag{45}$$

In the above expression tilde over quantities represents their comoving values. To estimate g_B and g_E, we need to know the electric and magnetic energy density in the matter dominated era after inflation and their evolution after reheating. The comoving spectral electric and magnetic field energy density in the matter dominated era before reheating ($\eta \le \eta_R$) for this case are [Sharma *et al.* [81]],

$$\frac{d\tilde{\rho}_B(k,\eta)}{d\ln k} = \begin{cases} D_{1h}\left(\frac{k}{k_p(\eta)}\right)^4 \left(\frac{\eta+\eta_R}{2\eta_R}\right)^{8\beta+2}, & k \le k_p(\eta) \\ D_{1h}\left(\frac{k}{k_p(\eta)}\right)^4 \left(\frac{\eta_k+\eta_R}{2\eta_R}\right)^{8\beta+2}, & k \ge k_p(\eta) \end{cases} \tag{46}$$

$$\frac{d\tilde{\rho}_E(k,\eta)}{d\ln k} = \begin{cases} D_{2h}\left(\frac{k}{k_p(\eta)}\right)^2 \left(\frac{\eta+\eta_R}{2\eta_R}\right)^{8\beta}, & k \le k_p(\eta) \\ D_{2h}\left(\frac{k}{k_p(\eta)}\right)^4 \left(\frac{\eta_k+\eta_R}{2\eta_R}\right)^{8\beta}, & k \ge k_p(\eta) \end{cases} \tag{47}$$

Here D_{1h} and D_{2h} are the amplitudes of spectral magnetic and electric energy densities at $k_0 = k_p(\eta_R)$ respectively. The values of D_{1h} and D_{2h} depend on the fraction of electromagnetic energy density to background energy density at reheating. We again consider GW production in two scenario on the basis of evolution of the magnetic field energy density after reheating.

After reheating, nonlinear processing (as in nonhelical case) of magnetic field spectrum takes place. However, the magnetic field energy density decays at a rate slower as compared to the case of nonhelical magnetic field because of the helicity conservation [87,88,95]. The evolution of the magnetic field for $\eta \ge \eta_R$ is given by,

$$\frac{d\tilde{\rho}_B(k)}{d\ln k} = \begin{cases} D_{1h}\left(\frac{k}{k_{NL}(\eta)}\right)^4 \left(\frac{\eta}{\eta_R}\right)^{-2/3}, & k \le k_{NL}(\eta) \\ D_{1h}\left(\frac{k}{k_{NL}(\eta)}\right)^{-2/3} \left(\frac{\eta}{\eta_R}\right)^{-2/3}, & k_\nu \ge k \ge k_{NL}(\eta) \end{cases} \tag{48}$$

Here,

$$k_{NL}(\eta) = k_0\left(\frac{\eta}{\eta_R}\right)^{-2/3} \tag{49}$$

By substituting Eqs. (46), (47), and (48) in Eq. (45), we estimate $\sum_{\aleph}|\Pi^{\aleph}|^2$ which we further substitute in Eq. (28) to calculate $\sum_{\aleph}|dh^{\aleph}/dx|^2$. After substituting $\sum_{\aleph}|dh^{\aleph}/dx|^2$ in Eq. (27) we calculate GW energy density spectrum for this case and the results are shown in Fig. 4. The peak value of the GW spectrum is 1.8×10^{-6} at the frequency 40 μHz for $T_R = 100$ GeV and 9.5×10^{-7} at the frequency 0.25 mHz for $T_R = 300$ GeV assuming $\epsilon = 1$ for both the cases. The peak values of the GW spectrum in this case is approximately twice the value in the case of nonhelical magnetic field. This is due to the fact that there is extra contribution to the GW spectrum which comes from the antisymmetric term in the two point correlation of the electric and magnetic field spectrum compare to the nonhelical case.

For the helical nature of the EM field, the generated GW spectrum is circularly polarized. Equation (43) and Eq. (44) suggest that the negatively polarized (-) mode dominates

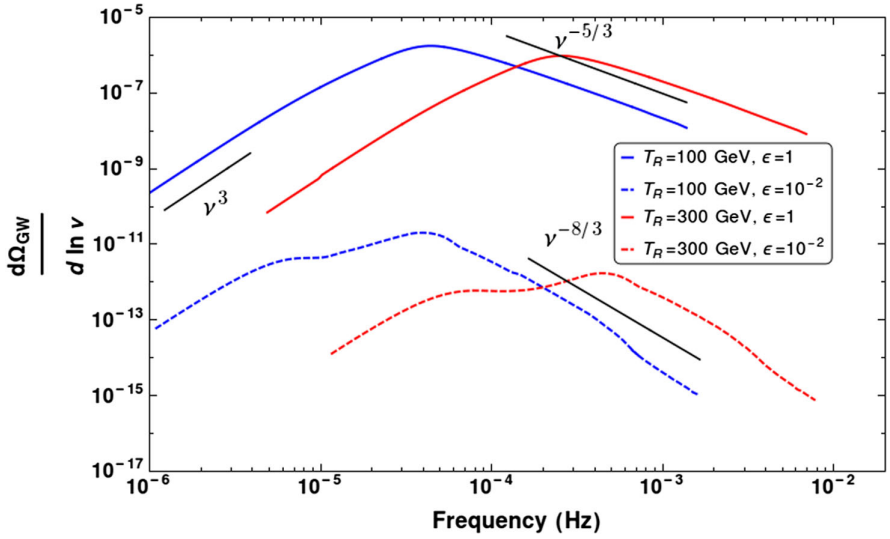

FIG. 4. In this figure we plot the GW energy spectrum generated from the EM field anisotropic stresses (helical case).

over the positively polarized (+) mode by an amount $h_E(k,\eta,\eta') + h_B(k,\eta,\eta')$. However the spectrum is unpolarized for the case when EM field is of nonhelical nature since the contribution of both the modes is equal as can be seen from Eq. (30). The sign of the GW polarization that dominates (+ or −), depends on the relative sign of the parity breaking term ($F_{\mu\nu}\tilde{F}^{\mu\nu}$) to the standard term ($F_{\mu\nu}F^{\mu\nu}$) in the EM field Lagrangian. In our analysis, we have taken both the terms with the same sign.

V. DETECTION OF THE GENERATED GW SPECTRUM WITH THE LISA

We now discuss the prospects of detection of the GW spectrum generated in our model with the LISA. For this, we calculate the signal to noise ratio (SNR) using the following definition [96],

$$\mathrm{SNR} \equiv \sqrt{T \int_{\nu_{\min}}^{\nu_{\max}} d\nu \left(\frac{d\Omega_{\mathrm{GW}}}{d \ln \nu} \Big/ \frac{d\Omega_n}{d \ln \nu} \right)^2}. \tag{50}$$

In the above expression, $d\Omega_n/d\ln\nu = (4\pi^2/3H_0^2)\nu^3 S_n(\nu)$ where $S_n(\nu)$ is the strain sensitivity of the LISA detector and T is the mission duration. The integration limits, $\nu_{\min}$ and $\nu_{\max}$, denote the minimal and maximal frequencies accessible at the LISA detector respectively. It is convenient to express the SNR as,

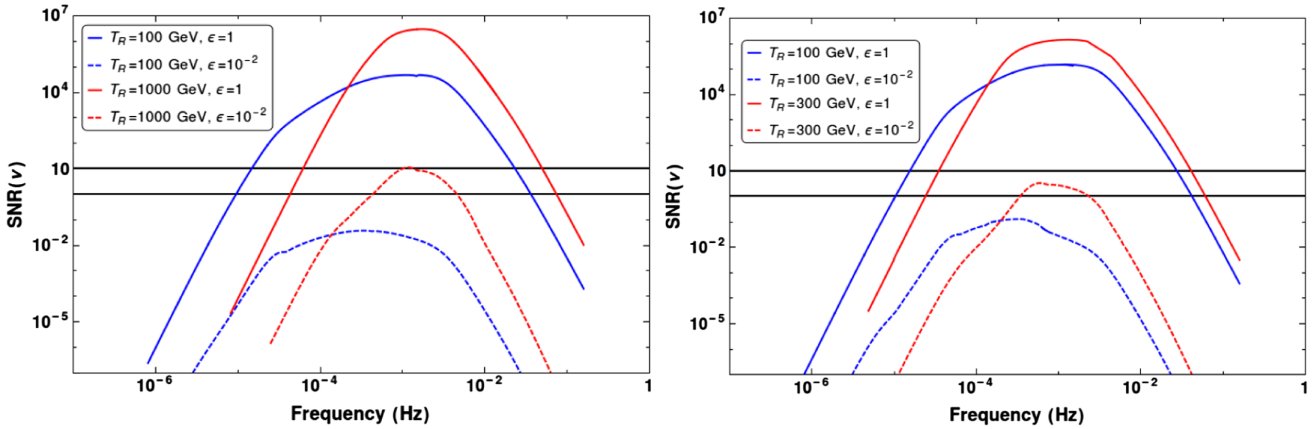

FIG. 5. In this figure, we plot SNR(ν) defined in Eq. (52) vs frequency for nonhelical and helical nature of the EM field. In the left panel, we plot SNR(ν) for the reheating scale $T_R = 100$ GeV and $T_R = 1000$ GeV and also for the different fraction (ϵ) of EM field energy density to the background energy density for nonhelical nature of EM field. In the right panel, we plot SNR(ν) for the reheating scale $T_R = 100$ GeV and $T_R = 300$ GeV and also for the different fraction (ϵ) of EM field energy density to the background energy density for helical nature of EM field. The lower and upper black horizontal lines represents SNR(ν) = 1 and SNR(ν) = 10, respectively. For these plots, we take $T = 3$ years.

$$\mathrm{SNR} = \sqrt{\int_{\nu_{\min}}^{\nu_{\max}} d\ln\nu \left(\sqrt{\nu T}\frac{d\Omega_{\mathrm{GW}}}{d\ln\nu} \Big/ \frac{d\Omega_n}{d\ln\nu}\right)^2} \equiv \sqrt{\int_{\nu_{\min}}^{\nu_{\max}} d\ln\nu (\mathrm{SNR}(\nu))^2}, \tag{51}$$

where

$$\mathrm{SNR}(\nu) = \sqrt{\nu T}\left(\frac{d\Omega_{\mathrm{GW}}}{d\ln\nu} \Big/ \frac{d\Omega_n}{d\ln\nu}\right). \tag{52}$$

Thus the square of the SNR(ν) provides the contribution to the value of square of the SNR per logarithmic frequency interval. To calculate the SNR for different reheating temperature T_R, we used the strain sensitivity $S_n(f)$ of a single channel of the LISA detector given in Eq. (2.4) in Caprini *et al.* [96].

In Fig. 5, we plot SNR(ν) with frequnecy (ν). This figure shows the sensitivity of the LISA detector for our generated GW spectrum in different frequency bands. In the Fig. 5, the lower and upper black horizontal lines represents $\mathrm{SNR}(\nu) = 1$ and $\mathrm{SNR}(\nu) = 10$, respectively. As evident from Fig. 5, the generated GW spectrum lies in the sensitivity range of LISA for our magnetic field generation models, in which ϵ is above a threshold value which depends on T_R. For $\epsilon = 10^{-2}$, the GW spectrum generated in our model can be detected with an $\mathrm{SNR} = 10$ for $T_R = 1000$ GeV in nonhelical case and $\mathrm{SNR} = 3$ for $T_R = 300$ GeV for helical case. In these estimates, we take $T = 3$ years. The value of SNR is even higher for large value of ϵ. Although, we show explicitly the GW spectrum only for $T_R = 100$ GeV and $T_R = 1000$ GeV for nonhelical case and $T_R = 100$ GeV and $T_R = 300$ GeV for helical case, the nature of the spectrum is qualitatively similar for other values of T_R.

VI. DISCUSSION AND CONCLUSION

Origin of large scale magnetic fields in the universe is a subject of intense study. An intriguing possibility is its generation during inflation with the model suggested by Turner and Widrow [47] and Ratra [48] being a popular scenario. However this model potentially suffers from what are known as the strong coupling and backreaction problems. In our earlier studies (Sharma *et al.* [80], Sharma *et al.* [81]), we suggested a model to address these issues. We showed that for a certain range of inflationary and reheating scales, it is possible to generate magnetic fields with the strengths of astrophysical interest while at the same time addressing all the difficulties raised regarding the models of Refs. [47,48]. Our models required a low energy scale of inflation and reheating, with $T_R < 5000$ GeV for magnetogenesis scenarios which generate nonhelical fields and $T_R < 500$ GeV for helical models [80,81]. They also predicted a blue spectrum peaked around the horizon scale of reheating with EM fields a significant fraction of the cosmological energy density at that epoch. These EM fields have nonzero anisotropic stresses which can source the production of a stochastic background of GW.

Here, we have therefore calculated the spectrum of the resulting stochastic GW background. Our aim was also to probe and constrain such models of inflationary magnetogenesis by examining whether the predicted GW spectrum can be detected by upcoming space mission LISA or PTA experiments. We obtained the GW spectrum for both magnetogenesis models where the generated EM fields are nonhelical or models which resulted in helical magnetic fields. Our results show that the strength of the generated GW in both nonhelical and helical cases are of similar order. However, in the case of helical EM fields, the generated GW spectrum is circularly polarized while it is unpolarized when the generated EM fields are nonhelical. All the scenarios in which reheating is above the 100 GeV scale produce a GW energy spectrum which lie in the sensitivity range of LISA provided that the fraction of EM field energy density to the background energy density (ϵ) is above a threshold value of order 10^{-2}. For $\epsilon = 10^{-2}$, the GW spectrum can be detected with an $\mathrm{SNR} = 10$ for $T_R = 1000$ GeV in nonhelical case and $\mathrm{SNR} = 3$ for $T_R = 300$ GeV for helical case. For these estimates of SNR, we assumed $T = 3$ years. The large value of ϵ gives larger value of SNR. For lower reheating temperature $T_R = 150$ MeV, the peak frequency shifts to 20 nano Hertz, where PTA experiments are more relevant. The current limits from PPTA constrain $\epsilon < 10^{-1}$ in this case.

An analytical estimate of the GW spectrum for low wave numbers and nonhelical fields is given by Eq. (39). The results of numerical integration are given in Fig. 3 when the source of GW are nonhelical primordial EM fields and in Fig. 4 for helical primordial fields, for some representative values of $T_R = 100$ GeV, $T_R = 300$ GeV, $T_R = 1000$ GeV and $T_R = 150$ MeV. Similar results can be obtained for other values of T_R. We also estimated these GW spectra for different fraction (ϵ) of EM field energy to the background energy density at reheating for each temperature scale.

The generated GW spectrum rises with wave number k as $d\Omega_{\mathrm{GW}}/d\ln(k) \propto k^3$, at low wave numbers. It remains almost k^3 until the wave number $k = k_{\mathrm{peak}}$ for the fraction of EM energy density to the background energy density at reheating, $\epsilon = 1$. However, for $\epsilon = 10^{-2}$, it changes to a spectrum $\propto k$. The GW spectrum then falls for the modes $k > k_{\mathrm{peak}}$ as $d\Omega_{\mathrm{GW}}/d\ln(k) \propto k^{-5/3}$ for $\epsilon = 1$ and $d\Omega_{\mathrm{GW}}/d\ln(k) \propto k^{-8/3}$ for $\epsilon = 10^{-2}$. This change in the slope of the spectrum for different ϵ could arise due to the fact that the turbulence correlation time is longer for a smaller ϵ. For $\epsilon = 1$, the peak value of the generated GW spectrum, $d\Omega_{\mathrm{GW}}/d\ln k \sim 4.1 \times 10^{-7}$ for the nonhelical case at $T_R = 1000$ GeV and $d\Omega_{\mathrm{GW}}/d\ln k \sim 9.5 \times 10^{-7}$

for the helical case at $T_R = 300$ GeV. The amplitude at the peak value decreases approximately as ϵ^2. Note that each wave number k can be converted into the frequency ν of the GW using $\nu = kc/2\pi$. The corresponding frequencies for these T_R is in mHz range where LISA is sensitive to detect a GW signal. The amplitude is similar for a lower value of T_R, but the frequency at which the GW spectrum peaks decreases as $\nu_{\rm peak} \propto T_R$ approximately.

Stochastic GW at these frequencies can also result from first order phase transitions at the corresponding temperatures. They are similar to the GW spectrum obtained here in some aspects but interestingly different in others. First, even the source spectra are not identical. The spectrum of the magnetic field generated during a phase transition is the same as ours for $k > k_0$ but for $k < k_0$, the spectrum is $\propto k^5$ (in our notation) instead of k^4. The other difference in the source spectrum is that in the case of phase transitions, all the modes are within the horizon unlike in our case where the magnetic field spectrum also has power in superhorizon modes. The GW spectrum obtained in the high frequency regime ($\nu > \nu_{\rm peak}$) sourced by magnetic field generated in phase transition is then similar to ours and also to the spectrum obtained in Niksa *et al.* [84]. It also agrees with the spectrum obtained in Pol *et al.* [92] via numerical simulation for $\epsilon \approx 10^{-2}$. In the low frequencies regime ($\nu < \nu_{\rm peak}$) for $\epsilon = 1$, we have obtained a spectrum $\propto \nu^3$ similar to the spectrum in phase transition scenario and also obtained by analytical estimate in Gogoberidze *et al.* [97]. However, in our case, this slope changes from k^3 to k around the peak as ϵ reduces from 1 to 10^{-2}, mainly due to a longer correlation for these modes.

The inflationary models considered in this work can also be distinguished from the signals arising in such first order phase transitions due to the following. As evident from the right panel of Fig. 2, there is a bump like feature around $\nu_{\rm peak}$ in the resultant GW energy spectrum for the more realistic case of $\epsilon = 10^{-2}$. This happens due to the fact that the contribution from the electric field anisotropic stresses before reheating dominates over the contribution from the magnetic field anisotropic stresses around the peak value of the spectrum and the total spectrum gets an additional contribution around the peak value. The GW spectrum generated during phase transition is also proportional to k^3 for the modes below the peak value and has another branch for the modes above the peak value developed due to Kolomogorov branch of the decaying magnetohydrodynamic turbulence. However, in the phase transition generated spectrum, there is no bump in these two branches around the peak value like in our case [92]. This feature is unique to our model of inflationary magnetogenesis. Another distinguishing feature of our model is the possibility of obtaining an almost fully circularly polarized stochastic GW background. A possible detection of GW by LISA or by PTA, with the features predicted here will provide an important probe of several models of inflationary magnetogenesis.

ACKNOWLEDGMENTS

R. S. and T. R. S. acknowledge the facilities at IUCAA Centre for Astronomy Research and Development (ICARD), University of Delhi. R. S. also acknowledges C.S.I.R., India for the financial support through Grant No. 09/045(1343)/2014-EMR-I. T. R. S. acknowledges the project grant from SERB EMR/2016/002286. The authors would like to thank Axel Brandenburg, Sukanta Bose, and Sanjit Mitra for useful discussions and helping out with LISA sensitivity curve. R. S. thanks Axel Brandenburg for hosting him at Nordita for the event "Gravitational Waves from the early universe", during which time a part of this work was done.

APPENDIX A: CALCULATION TO ESTIMATE d_1 AND d_2

To calculate d_1 and d_2 given in Eq. (15), we match $h^{\aleph}$ and its derivative at the epoch of reheating ($\eta = \eta_R$). The matching relations are,

$$h^{\aleph}(w_R) = h^{\aleph}(x_R)$$
$$\left.\frac{dh^{\aleph}(w)}{dw}\right|_{w=w_R} = \left.\frac{dh^{\aleph}(x)}{dx}\right|_{x=x_R} \tag{A1}$$

Here, $w_R = 2k\eta_R$ and $x_R = k\eta_R$ which implies $w_R = 2x_R$. Using Eq. (13) and Eq. (15), the above two conditions imply,

$$d_1 = \frac{1}{32x_R^3}\left(\left(\int_{w_i}^{2x_R}\frac{12\Pi^{\aleph}(w_1)(\sin w_1 - w_1\cos w_1)}{w_1}dw_1\right)(-8x_R^2\cos x_R + 4x_R\sin x_R + \cos x_R + \cos 3x_R) + (8x_R^2\sin x_R + 4x_R\cos x_R - \sin x_R - \sin 3x_R) \times \left(\int_{w_i}^{2x_R}\frac{12\Pi^{\aleph}(w_1)(w_1\sin w_1 + \cos w_1)}{w_1}dw_1\right)\right) \tag{A2}$$

$$d_2 = \frac{1}{32x_R^3}\left(\left(\int_{w_i}^{2x_R}\frac{12\Pi^{\aleph}(w_1)(\sin w_1 - w_1\cos w_1)}{w_1}dw_1\right)(8x_R^2\sin x_R + 4x_R\cos x_R - \sin x_R + \sin 3x_R) + (8x_R^2\cos x_R - 4x_R\sin x_R - \cos x_R + \cos 3x_R) \times \left(\int_{w_i}^{2x_R}\frac{12\Pi^{\aleph}(w_1)(w_1\sin w_1 + \cos w_1)}{w_1}dw_1\right)\right). \tag{A3}$$

Since we are interested in the production of GW from the EM field anisotropic stress, we neglect the homogeneous part in the $h^{\aleph}$ expression for matter dominance given in Eq. (13) while calculating the above expressions. Using Eq. (15), we get the following expression for $dh^{\aleph}/dx$,

$$\frac{dh^{\aleph}(\vec{k},x)}{dx} = d_1\left(\frac{\cos x}{x} - \frac{\sin x}{x^2}\right) + d_2\left(\frac{\sin x}{x} - \frac{\cos x}{x^2}\right) - 4\left(\frac{\cos x}{x} - \frac{\sin x}{x^2}\right)\int_{x_R}^{x} dx_1\Pi^{\aleph}(\vec{k},x_1) \times y_0(x_1) + 4\left(\frac{\sin x}{x} - \frac{\cos x}{x^2}\right)\int_{x_R}^{x} dx_1\Pi^{\aleph}(\vec{k},x_1)j_0(x_1) \tag{A4}$$

To estimate the GW spectrum, we need to calculate $|dh^{\aleph}/dx|^2$. After multiplying the above expression with its complex conjugate and taking the limit $x \gg 1$ (since we are interested in the modes which are deep inside the Hubble radius at the present epoch), we get,

$$\left|\frac{dh^{\aleph}}{dx}\right|^2(k,x) = |d_1|^2\left(\frac{\sin x}{x}\right)^2 + |d_2|^2\left(\frac{\cos x}{x}\right)^2 + (d_1d_2^* + d_1^*d_2)\frac{\sin x\cos x}{x^2} + \frac{8}{x^2}\int_{x_R}^{x}dx_1\int_{x_R}^{x}dx_2|\Pi^{\aleph}|^2(k,x_1,x_2)\frac{\cos(x_2-x_1)+\cos(2x-x_1-x_2)}{x_1x_2} \tag{A5}$$

In the above expression, we only keep the terms proportional to $(1/x)^2$ and neglect the terms which have higher power of $1/x$ as those terms are subdominant in the limit $x \gg 1$. After reheating, the source term contributes until the epoch of neutrino decoupling. This is because anisotropic stress due to neutrinos comes into picture after neutrino decoupling and they balance the magnetic field anisotropic stress. Hence, there is no contribution to the GW energy density after neutrino decoupling. Further, averaging the above expression over a timescale greater than the time period of oscillation, we get,

$$\left|\frac{dh^{\aleph}}{dx}\right|^2(k,x) = \frac{1}{2x^2}(|d_1|^2 + |d_2|^2) + \frac{8}{x^2}\int_{x_R}^{x_{\nu d}}\int_{x_R}^{x_{\nu d}}dx_1dx_2|\Pi^{\aleph}|^2(k,x_1,x_2)\frac{\cos(x_2-x_1)}{x_1x_2} \tag{A6}$$

APPENDIX B: CALCULATION FOR THE ESTIMATE OF GW ENERGY SPECTRUM

Here, we provide the calculation for analytical estimate of the GW energy spectrum for the modes $k < k_H$ given in Eq. (39). To evaluate GW energy spectrum, we estimate $|dh^{\aleph}/dx|^2(k,x)$ given in Eq. (A6),

$$\left|\frac{dh^{\aleph}}{dx}\right|^2(k,x) = \frac{1}{2x^2}(|d_1|^2 + |d_2|^2) + \frac{8}{x^2}\int_{x_R}^{x_{\nu d}}\int_{x_R}^{x_{\nu d}}dx_1dx_2|\Pi^{\aleph}|^2(k,x_1,x_2)\frac{\cos(x_2-x_1)}{x_1x_2} \tag{B1}$$

In the above expression, the first part in the rhs denotes the contribution before reheating and the second part denotes the contribution after reheating. In the postinflationary matter dominated era both electric and magnetic field anisotropic stresses contribute in the production of GW. After reheating, only magnetic field anisotropic stresses contribute as electric fields get shorted out due to the large conductivity of the relativistic plasma.

1. Calculation for the contribution before reheating

For $k < k_H = k_0/\beta$, $x_R = k\eta_R < 1$. In this limit, the expression for d_1 and d_2 given in Eq. (A2) and Eq. (A3) respectively, reduces to,

$$d_1 = \frac{3}{8x_R^3}\left(2\int_{w_i}^{2x_R}\frac{w_1^2}{3}\Pi^{\aleph}(w_1)dw_1 + \frac{32x_R^3}{3}\int_{w_i}^{2x_R}\frac{1}{w_1}\Pi^{\aleph}(w_1)dw_1\right)$$
$$d_2 = \frac{3}{8x_R^3}\left(-\frac{32x_R^6}{45}\int_{w_i}^{2x_R}\frac{1}{w_1}\Pi^{\aleph}(w_1)dw_1 + 6x_R\int_{w_i}^{2x_R}\frac{w_1^2}{3}\Pi^{\aleph}(w_1)dw_1\right). \tag{B2}$$

Further the expression for $|d_1|^2$ and $|d_2|^2$ is given by,

$$|d_1|^2 = \frac{9}{64x_R^6}\left(\int_{w_i}^{2x_R}\int_{w_i}^{2x_R}\left(\frac{4w_1^2w_2^2}{9} + \frac{1024x_R^6}{9w_1w_2} + \frac{64x_R^3(\frac{w_1^2}{w_2}+\frac{w_2^2}{w_1})}{9}\right)|\Pi^{\aleph}|^2(k,w_1,w_2)dw_1dw_2\right)$$
$$|d_2|^2 = \frac{9}{64x_R^6}\left(36x_R^2\int_{w_i}^{2x_R}\int_{w_i}^{2x_R}\frac{w_1^2w_2^2}{9}|\Pi^{\aleph}|^2(k,w_1,w_2)dw_1dw_2\right).$$

In the expression of $|d_2|^2$, we neglect the contribution from the first term in the expression of d_2 since this term is much smaller than the second term in the limit $x_R < 1$. After substituting $|\Pi^{\aleph}|^2$ from Eq. (30), we get

$$|d_1|^2 = \frac{9}{8x_R^2}\left(\frac{1}{\tilde{\rho}+\tilde{p}}\right)^2\left(\int_{w_i}^{2x_R}\int_{w_i}^{2x_R}\left(\frac{4w_1^2w_2^2}{9} + \frac{1024x_R^6}{9w_1w_2} + \frac{64x_R^3(\frac{w_1^2}{w_2}+\frac{w_2^2}{w_1})}{9}\right)\left(\frac{1}{w_1^2w_2^2}\right)\right.$$
$$\left.\times\,(f_B(k,w_1,w_2)+f_E(k,w_1,w_2))dw_1dw_2\right). \tag{B3}$$

To evaluate the above expression, we first calculate $f_B(k,w_1,w_2)+f_E(k,w_1,w_2)$. Substituting Eq. (31) in Eq. (22), we get,

$$f_B(k,w_1,w_2)+f_E(k,w_1,w_2) = \pi^2\int_0^{\infty}\frac{dq}{q}\int_{-1}^{1}d\gamma\left[\frac{d\tilde{\rho}_B(q,w_1)}{d\ln q}\frac{d\tilde{\rho}_B(|\vec{k}-\vec{q}|,w_1)}{d\ln|\vec{k}-\vec{q}|}C_B(q,w_1,w_2)\right.$$
$$\times C_B(|\vec{k}-\vec{q}|,w_1,w_2) + \frac{d\tilde{\rho}_E(q,w_1)}{d\ln q}\frac{d\tilde{\rho}_E(|\vec{k}-\vec{q}|,w_1)}{d\ln|\vec{k}-\vec{q}|}C_E(q,w_1,w_2)$$
$$\left.\times\,C_E(|\vec{k}-\vec{q}|,w_1,w_2)\right](1+\gamma^2+\beta^2+\gamma^2\beta^2). \tag{B4}$$

It is evident from Eq. (32) and Eq. (33) that the magnetic and electric spectral energy densities decay rapidly for $k \geq k_p(\eta)$. Keeping this in mind, we neglect the contribution of magnetic and electric power spectra for $k \geq k_p(\eta)$. Further, we take the upper limit of the q integration to be k_0 instead of $k_p(\eta)$ because within one Hubble expansion time electric and magnetic field spectral energy densities increase by a very large value. The most of the contribution in the above integral is near the epoch of reheating. Hence, taking k_0 instead k_p will not change our result much. Using Eq. (32) and Eq. (33), the above expression reduces to,

$$f_B(k,w_1,w_2)+f_E(k,w_1,w_2) = \pi^2\int_0^{k_0}\frac{dq}{q}\int_{-1}^{1}d\gamma\left[D_1^2\left(\frac{q}{k_0}\right)^4\frac{(k^2+q^2-2kq\gamma)^{1/2}}{k_0^4}\left(\frac{w_1w_2}{(2x_R)^2}\right)^{8\beta+2}\right.$$
$$\left.+\,D_2^2\left(\frac{q}{k_0}\right)^2\frac{(k^2+q^2-2kq\gamma)^{-1/2}}{k_0^2}\left(\frac{w_1w_2}{(2x_R)^2}\right)^{8\beta}\right](1+\gamma^2+\beta^2+\gamma^2\beta^2). \tag{B5}$$

To solve the above expression, we first calculate the γ integral as,

$$\int_{-1}^{1}d\gamma(k^2+q^2-2kq\gamma)^{1/2}(1+\gamma^2+\beta^2+\gamma^2\beta^2) = \begin{cases}\frac{8(5k^4+72k^2q^2+147q^4)}{315q^3}, & k\leq q\\ \frac{16(105k^6+6k^2q^4+q^6)}{315k^5}, & k\geq q\end{cases}$$
$$\int_{-1}^{1}d\gamma(k^2+q^2-2kq\gamma)^{-1/2}(1+\gamma^2+\beta^2+\gamma^2\beta^2) = \begin{cases}\frac{8(k^2+49q^2)}{105q^3}, & k\leq q\\ \frac{16(35k^4-72k^2q^2-3q^4)}{105k^5}, & k\geq q\end{cases}$$

Further, we divide the q integral into two parts, $\int_0^{k_0} dq = \int_0^k dq + \int_k^{k_0} dq$ and evaluate each of the part separately. We get,

$$\int_0^{k_0} \frac{dq}{q} \int_{-1}^{1} d\gamma \left(\frac{q}{k_0}\right)^4 \frac{(k^2+q^2-2kq\gamma)^{1/2}}{k_0^4}(1+\gamma^2+\beta^2+\gamma^2\beta^2) = \frac{8}{1575k_0^8}(25k^4k_0+120k^2k_0^3+147k_0^5-21k^5)$$
$$\int_0^{k_0} \frac{dq}{q} \int_{-1}^{1} d\gamma \left(\frac{q}{k_0}\right)^2 \frac{(k^2+q^2-2kq\gamma)^{-1/2}}{k_0^2}(1+\gamma^2+\beta^2+\gamma^2\beta^2) = \frac{4(98k_0^2-2k^2-35kk_0)}{105k_0^5} \tag{B6}$$

After taking only the contribution from the dominating terms, we get,

$$f_B(k,w_1,w_2)+f_E(k,w_1,w_2) = \pi^2\left[D_1^2\frac{56}{75k_0^3}\left(\frac{w_1w_2}{(2x_R)^2}\right)^{8\beta+2} + D_2^2\frac{56}{15k_0^3}\left(\frac{w_1w_2}{(2x_R)^2}\right)^{8\beta}\right]. \tag{B7}$$

Since during the postinflationary matter dominated era, the electric spectral energy density dominates over the magnetic spectral energy density, $D_1 < D_2$, the quantity $(w_1w_2/(2x_R)^2)$ is always less than unity. Therefore we neglect the first term in comparison to the second term in the above expression. This implies,

$$f_B(k,w_1,w_2)+f_E(k,w_1,w_2) = \pi^2\left[D_2^2\frac{56}{15k_0^3}\left(\frac{w_1w_2}{(2x_R)^2}\right)^{8\beta}\right]. \tag{B8}$$

After substituting the above expression in Eq. (B3) and using new variables for integration defined as $z_1 = w_1/(2x_R)$ and $z_2 = w_2/(2x_R)$, we get

$$|d_1|^2 = \frac{9\pi^2D_2^2}{2}\frac{56}{15k_0^3}\left(\frac{1}{\tilde{\rho}+\tilde{p}}\right)^2\int_{z_i}^{1}\int_{z_i}^{1}\left(\frac{4}{9}+\frac{16}{9z_1^3z_2^3}+\frac{8}{9}\left(\frac{1}{z_1^3}+\frac{1}{z_2^3}\right)\right)(z_1z_2)^{8\beta}dz_1dz_2. \tag{B9}$$

After calculating the above integral we get,

$$|d_1|^2 = \frac{9\pi^2D_2^2}{2}\frac{56}{15k_0^3}\left(\frac{1}{\tilde{\rho}+\tilde{p}}\right)^2\frac{64\beta^2}{(1-4\beta)^2(8\beta+1)^2}. \tag{B10}$$

Similarly we can calculate the expression for $|d_2|^2$,

$$|d_2|^2 = \frac{9\pi^2D_2^2}{2}\frac{56}{15k_0^3}\left(\frac{1}{\tilde{\rho}+\tilde{p}}\right)^2\frac{4x_R^2}{(8\beta+1)^2}. \tag{B11}$$

From the above expression of $|d_1|^2$ and $|d_2|^2$, we see that $|d_1|^2$ is larger than $|d_2|^2$ for $x_R < 1$. Therefore we neglect the contribution from $|d_2|^2$ in our further calculation. After substituting $|d_1|^2$ in Eq. (B1), we get

$$\left|\frac{dh^{\aleph}}{dx}\right|^2(k,x) = \frac{42\pi^2}{5x^2}\left(\frac{1}{k_0}\right)^3\left(\frac{D_2}{\tilde{\rho}+\tilde{p}}\right)^2\left(\frac{64\beta^2}{(1-4\beta)^2(8\beta+1)^2}\right). \tag{B12}$$

Further substituting the above expression in Eq. (27), we obtain the following expression for the GW energy spectrum,

$$\left.\frac{d\Omega_{\rm GW}}{d\ln k}\right|_0 = \frac{7\Omega_R}{5}\left(\frac{k}{k_0}\right)^3\left(\frac{D_2}{\tilde{\rho}+\tilde{p}}\right)^2\left(\frac{64\beta^2}{(1-4\beta)^2(8\beta+1)^2}\right). \tag{B13}$$

2. Calculation for the contribution after reheating

To evaluate GW energy spectrum after reheating, we estimate $|dh^{\aleph}/dx|^2(k,x)$ given in Eq. (B1),

$$\left|\frac{dh^{\aleph}}{dx}\right|^2_{x>x_R}(k,x) = \frac{8}{x^2}\int_{x_R}^{x_{vd}}\int_{x_R}^{x_{vd}} dx_1 dx_2 |\Pi^{\aleph}|^2(k,x_1,x_2)\frac{\cos(x_2-x_1)}{x_1 x_2}. \tag{B14}$$

After substituting $|\Pi^{\aleph}|^2$ from Eq. (30), we get

$$\left|\frac{dh^{\aleph}}{dx}\right|^2_{x>x_R}(k,x) = \frac{4}{x^2}\left(\frac{1}{\tilde{\rho}+\tilde{p}}\right)^2\int_{x_R}^{x_{vd}}\int_{x_R}^{x_{vd}} dx_1 dx_2 f_B(k,w_1,w_2)\frac{\cos(x_2-x_1)}{x_1 x_2}. \tag{B15}$$

To evaluate the above expression, we first calculate $f_B(k,w_1,w_2)$. Substituting Eq. (31) in Eq. (22), we get,

$$f_B(k,x_1,x_2) = \pi^2\int_0^\infty \frac{dq}{q}\int_{-1}^{1} d\gamma \frac{d\tilde{\rho}_B(q,x_1)}{d\ln q}\frac{1}{(|\vec{k}-\vec{q}|)^3}\frac{d\tilde{\rho}_B(|\vec{k}-\vec{q}|,x_1)}{d\ln|\vec{k}-\vec{q}|}C_B(q,x_1,x_2)C_B(|\vec{k}-\vec{q}|,x_1,x_2)(1+\gamma^2+\beta^2+\gamma^2\beta^2). \tag{B16}$$

Using Eqs. (B15), (B16) and (27), we get

$$\begin{aligned}\left.\frac{d\Omega_{\rm GW}}{d\ln k}\right|_0 = {}& \frac{2\Omega_R}{3(\tilde{\rho}+\tilde{p})^2}k^3\int_{x_R}^{x_{vd}}\int_{x_R}^{x_{vd}} dx_1 dx_2\frac{\cos(x_2-x_1)}{x_1 x_2}\int_0^\infty\frac{dq}{q}\int_{-1}^{1}d\gamma\frac{d\tilde{\rho}_B(q,x_1)}{d\ln q}\frac{1}{(|\vec{k}-\vec{q}|)^3}\frac{d\tilde{\rho}_B(|\vec{k}-\vec{q}|,x_1)}{d\ln|\vec{k}-\vec{q}|}\\ &\times C_B(q,x_1,x_2)C_B(|\vec{k}-\vec{q}|,x_1,x_2)(1+\gamma^2+\beta^2+\gamma^2\beta^2).\end{aligned} \tag{B17}$$

The magnetic energy spectrum peaks at $k=k_{NL}$, the main contribution to the integral comes when $q\sim k_{NL}$ and $|\vec{k}-\vec{q}|\sim k_{NL}$. For the case $k\ll k_{NL}$, $|\vec{k}-\vec{q}|\sim q$ and C_B changes from 1 to a small value within one Hubble time. Therefore the dominant contribution comes within one Hubble time from reheating.

$$\begin{aligned}\left.\frac{d\Omega_{\rm GW}}{d\ln k}\right|_0 &\approx \frac{2\Omega_R}{3(\tilde{\rho}+\tilde{p})^2}k^3\int_{x_R}^{2x_R}\int_{x_R}^{2x_R} dx_1 dx_2\frac{\cos(x_2-x_1)}{x_1 x_2}\left[\frac{D_1^2}{k_{NL}^3}\left(\frac{x_1}{x_R}\right)^{-4/3}\left(\frac{x_1}{x_R}\right)^{-4/3}\right]C_B(k_{NL},x_1,x_2)^2\\ &\quad\times\int_{-1}^{1}d\gamma(1+\gamma^2+\gamma^2+\gamma^4)\\ &= \frac{56}{15}\frac{2\Omega_R}{3}\left(\frac{D_1}{\tilde{\rho}+\tilde{p}}\right)^2\left(\frac{k}{k_0}\right)^3\int_{x_R}^{2x_R}\int_{x_R}^{2x_R} dx_1 dx_2\frac{\cos(x_2-x_1)}{x_1 x_2}\left(\frac{x_1}{x_R}\right)^{-4/3}\left(\frac{x_1}{x_R}\right)^{-4/3}C_B(k_{NL},x_1,x_2)^2.\end{aligned}$$

In terms of the variable $z_1=x_1/x_R$ and $z_2=x_2/x_R$, the above expression reduces to,

$$\left.\frac{d\Omega_{\rm GW}}{d\ln k}\right|_0 \approx \frac{56}{15}\frac{2\Omega_R}{3}\left(\frac{D_1}{\tilde{\rho}+\tilde{p}}\right)^2\left(\frac{k}{k_0}\right)^3\int_1^2\int_1^2 dz_1 dz_2\frac{\cos(x_R^2(z_2-z_1))}{z_1 z_2}(z_1)^{-8/3}(z_1)C_B(k_{NL},z_1,z_2)^2.$$

The modes $k<k_H$ are outside the Hubble horizon at reheating. For these modes, $x_R<1$ so we can approximate $\cos(x_R^2(z_2-z_1))\sim 1$ for these modes. Using this, the GW spectrum for the modes $k<k_H$, we get,

$$\begin{aligned}\left.\frac{d\Omega_{\rm GW}}{d\ln k}\right|_0 &\approx \frac{56}{15}\frac{2\Omega_R}{3}\left(\frac{D_1}{\tilde{\rho}+\tilde{p}}\right)^2\left(\frac{k}{k_0}\right)^3\int_1^2\int_1^2\frac{dz_1 dz_2}{z_1 z_2}z_1^{-8/3}z_1 C_B(k_{NL},z_1,z_2)^2\\ &= c\Omega_R\left(\frac{D_1}{\tilde{\rho}+\tilde{p}}\right)^2\left(\frac{k}{k_0}\right)^3\end{aligned} \tag{B18}$$

where,

$$c = \frac{56}{15}\frac{2}{3}\int_1^2\int_1^2\frac{dz_1 dz_2}{z_1 z_2}(z_1)^{-8/3}z_1 C_B(k_{NL},z_1,z_2)^2$$

which has different value for different k_{NL} and ϵ since unequal time correlation function, C_B depends upon k_{NL} and ϵ. For $T_R = 100$ GeV and $\epsilon = 1$, $c = 0.18$. As is evident from the above expression, GW energy spectrum is proportional to k^3 and to the fraction of magnetic field energy density to the background energy density for the modes $k < k_H$.

[1] B. P. Abbott *et al.* (Virgo and LIGO Scientific Collaborations), Phys. Rev. Lett. **116**, 061102 (2016).
[2] B. P. Abbott *et al.* (Virgo and LIGO Scientific Collaborations), Phys. Rev. Lett. **116**, 241103 (2016).
[3] B. P. Abbott *et al.* (Virgo and LIGO Scientific Collaborations), Phys. Rev. Lett. **118**, 221101 (2017); **121**, 129901(E) (2018).
[4] B. P. Abbott *et al.* (Virgo and LIGO Scientific Collaborations), Astrophys. J. **851**, L35 (2017).
[5] B. P. Abbott *et al.* (Virgo and LIGO Scientific Collaborations), Phys. Rev. Lett. **119**, 141101 (2017).
[6] A. H. Guth, Phys. Rev. D **23**, 347 (1981); Adv. Ser. Astrophys. Cosmol. **3**, 139 (1987).
[7] A. H. Guth and S. Y. Pi, Phys. Rev. Lett. **49**, 1110 (1982).
[8] J. M. Bardeen, P. J. Steinhardt, and M. S. Turner, Phys. Rev. D **28**, 679 (1983).
[9] V. A. Rubakov, M. V. Sazhin, and A. V. Veryaskin, Phys. Lett. **115B**, 189 (1982).
[10] A. A. Starobinskii, Sov. Astron. Lett. **9**, 302 (1983).
[11] Y. Akrami *et al.* (Planck Collaboration), Astrophys. Space Sci. **364**, 69 (2019).
[12] L. Randall and G. Servant, J. High Energy Phys. 05 (2007) 054.
[13] R. Durrer and M. Ruser, Phys. Rev. Lett. **99**, 071601 (2007).
[14] R. Durrer, M. Kunz, and A. Melchiorri, Phys. Rev. D **59**, 123005 (1999).
[15] C. J. Hogan, Mon. Not. R. Astron. Soc. **218**, 629 (1986).
[16] A. Kosowsky, M. S. Turner, and R. Watkins, Phys. Rev. D **45**, 4514 (1992).
[17] A. Kosowsky, M. S. Turner, and R. Watkins, Phys. Rev. Lett. **69**, 2026 (1992).
[18] A. Kosowsky and M. S. Turner, Phys. Rev. D **47**, 4372 (1993).
[19] M. Kamionkowski, A. Kosowsky, and M. S. Turner, Phys. Rev. D **49**, 2837 (1994).
[20] C. Caprini, R. Durrer, and G. Servant, Phys. Rev. D **77**, 124015 (2008).
[21] S. J. Huber and T. Konstandin, J. Cosmol. Astropart. Phys. 09 (2008) 022.
[22] C. Caprini, R. Durrer, T. Konstandin, and G. Servant, Phys. Rev. D **79**, 083519 (2009).
[23] A. Kosowsky, A. Mack, and T. Kahniashvili, Phys. Rev. D **66**, 024030 (2002).
[24] A. D. Dolgov, D. Grasso, and A. Nicolis, Phys. Rev. D **66**, 103505 (2002).
[25] C. Caprini and R. Durrer, Phys. Rev. D **74**, 063521 (2006).
[26] G. Gogoberidze, T. Kahniashvili, and A. Kosowsky, Phys. Rev. D **76**, 083002 (2007).
[27] A. Megevand, Phys. Rev. D **78**, 084003 (2008).
[28] T. Kahniashvili, L. Campanelli, G. Gogoberidze, Y. Maravin, and B. Ratra, Phys. Rev. D **78**, 123006 (2008); **79**, 109901(E) (2009).
[29] C. Caprini and R. Durrer, Phys. Rev. D **65**, 023517 (2001).
[30] T. Kahniashvili, L. Kisslinger, and T. Stevens, Phys. Rev. D **81**, 023004 (2010).
[31] R. Apreda, M. Maggiore, A. Nicolis, and A. Riotto, Nucl. Phys. **B631**, 342 (2002).
[32] A. Nicolis, Classical Quantum Gravity **21**, L27 (2004).
[33] C. Grojean and G. Servant, Phys. Rev. D **75**, 043507 (2007).
[34] K. Jedamzik, M. Lemoine, and J. Martin, J. Cosmol. Astropart. Phys. (2010) 021.
[35] D. Jimnez, K. Kamada, K. Schmitz, and X.-J. Xu, J. Cosmol. Astropart. Phys. 12 (2017) 011.
[36] J. Liu, Z.-K. Guo, R.-G. Cai, and G. Shiu, Phys. Rev. D **99**, 103506 (2019).
[37] T. Kahniashvili, G. Gogoberidze, and B. Ratra, Phys. Rev. Lett. **100**, 231301 (2008).
[38] G. Gogoberidze, T. Kahniashvili, and A. Kosowsky, Phys. Rev. D **76**, 083002 (2007).
[39] T. Kahniashvili, G. Gogoberidze, and B. Ratra, Phys. Rev. Lett. **95**, 151301 (2005).
[40] S. Anand, J. R. Bhatt, and A. K. Pandey, Eur. Phys. J. C **79**, 119 (2019).
[41] R. Beck, Space Sci. Rev. **99**, 243 (2001).
[42] T. E. Clarke, P. P. Kronberg, and H. Boehringer, Astrophys. J. **547**, L111 (2001).
[43] L. M. Widrow, Rev. Mod. Phys. **74**, 775 (2002).
[44] A. Neronov and I. Vovk, Science **328**, 73 (2010).
[45] A. M. Taylor, I. Vovk, and A. Neronov, Astron. Astrophys. **529**, A144 (2011).
[46] K. Subramanian, Galaxies **7**, 47 (2019).
[47] M. S. Turner and L. M. Widrow, Phys. Rev. D **37**, 2743 (1988).
[48] B. Ratra, Astrophys. J. **391**, L1 (1992).
[49] K. Takahashi, K. Ichiki, H. Ohno, and H. Hanayama, Phys. Rev. Lett. **95**, 121301 (2005).
[50] R. Gopal and S. Sethi, Mon. Not. R. Astron. Soc. **363**, 521 (2005).
[51] J. Martin and J. Yokoyama, J. Cosmol. Astropart. Phys. 01 (2008) 025.
[52] L. Campanelli, P. Cea, G. L. Fogli, and L. Tedesco, Phys. Rev. D **77**, 043001 (2008).
[53] R. Durrer, L. Hollenstein, and R. K. Jain, J. Cosmol. Astropart. Phys. 03 (2011) 037.
[54] I. Agullo and J. Navarro-Salas, arXiv:1309.3435.
[55] R. J. Z. Ferreira, R. K. Jain, and M. S. Sloth, J. Cosmol. Astropart. Phys. 10 (2013) 004.

[56] C. Caprini and L. Sorbo, J. Cosmol. Astropart. Phys. 10 (2014) 056.
[57] T. Kobayashi, J. Cosmol. Astropart. Phys. 05 (2014) 040.
[58] K. Atmjeet, I. Pahwa, T. R. Seshadri, and K. Subramanian, Phys. Rev. D **89**, 063002 (2014).
[59] K. Atmjeet, T. R. Seshadri, and K. Subramanian, Phys. Rev. D **91**, 103006 (2015).
[60] L. Sriramkumar, K. Atmjeet, and R. K. Jain, J. Cosmol. Astropart. Phys. 09 (2015) 010.
[61] L. Campanelli, Eur. Phys. J. C **75**, 278 (2015).
[62] G. Tasinato, J. Cosmol. Astropart. Phys. 03 (2015) 040.
[63] J. R. Bhatt and A. K. Pandey, Phys. Rev. D **94**, 043536 (2016).
[64] D. Chowdhury, L. Sriramkumar, and R. K. Jain, Phys. Rev. D **94**, 083512 (2016).
[65] T. Fujita and R. Namba, Phys. Rev. D **94**, 043523 (2016).
[66] S. Mukohyama, Phys. Rev. D **94**, 121302 (2016).
[67] S. Chakraborty, S. Pal, and S. SenGupta, arXiv:1810.03478.
[68] T. Fujita and R. Durrer, J. Cosmol. Astropart. Phys. 09 (2019) 008.
[69] T. Vachaspati, Phys. Lett. B **265**, 258 (1991).
[70] G. Sigl, A. V. Olinto, and K. Jedamzik, Phys. Rev. D **55**, 4582 (1997).
[71] L. S. Kisslinger, Phys. Rev. D **68**, 043516 (2003).
[72] A. G. Tevzadze, L. Kisslinger, A. Brandenburg, and T. Kahniashvili, Astrophys. J. **759**, 54 (2012).
[73] L. Biermann, Z. Naturforsch. A **5**, 65 (1950).
[74] E. Fenu, C. Pitrou, and R. Maartens, Mon. Not. R. Astron. Soc. **414**, 2354 (2011).
[75] K. Subramanian, D. Narasimha, and S. M. Chitre, Mon. Not. R. Astron. Soc. **271**, L15 (1994).
[76] N. Y. Gnedin, A. Ferrara, and E. G. Zweibel, Astrophys. J. **539**, 505 (2000).
[77] R. M. Kulsrud, R. Cen, J. P. Ostriker, and D. Ryu, Astrophys. J. **480**, 481 (1997).
[78] V. Demozzi, V. Mukhanov, and H. Rubinstein, J. Cosmol. Astropart. Phys. 08 (2009) 025.
[79] T. Kobayashi and N. Afshordi, J. High Energy Phys. 10 (2014) 166.
[80] R. Sharma, S. Jagannathan, T. R. Seshadri, and K. Subramanian, Phys. Rev. D **96**, 083511 (2017).
[81] R. Sharma, K. Subramanian, and T. R. Seshadri, Phys. Rev. D **97**, 083503 (2018).
[82] C. Caprini, R. Durrer, and T. Kahniashvili, Phys. Rev. D **69**, 063006 (2004).
[83] K. Subramanian, Astron. Nachr. **331**, 110 (2010).
[84] P. Niksa, M. Schlederer, and G. Sigl, Classical Quantum Gravity **35**, 144001 (2018).
[85] A. Lewis, Phys. Rev. D **70**, 043011 (2004).
[86] R. Sharma and S. Singh, Phys. Rev. D **96**, 025012 (2017).
[87] K. Subramanian, Rep. Prog. Phys. **79**, 076901 (2016).
[88] R. Banerjee and K. Jedamzik, Phys. Rev. D **70**, 123003 (2004).
[89] A. Brandenburg, T. Kahniashvili, and A. G. Tevzadze, Phys. Rev. Lett. **114**, 075001 (2015).
[90] A. Brandenburg and T. Kahniashvili, Phys. Rev. Lett. **118**, 055102 (2017).
[91] J. Zrake, Astrophys. J. **794**, L26 (2014).
[92] A. R. Pol, S. Mandal, A. Brandenburg, T. Kahniashvili, and A. Kosowsky, arXiv:1903.08585.
[93] P. F. de Salas, M. Lattanzi, G. Mangano, G. Miele, S. Pastor, and O. Pisanti, Phys. Rev. D **92**, 123534 (2015).
[94] P. D. Lasky *et al.*, Phys. Rev. X **6**, 011035 (2016).
[95] M. Christensson, M. Hindmarsh, and A. Brandenburg, Phys. Rev. E **64**, 056405 (2001).
[96] C. Caprini, D. G. Figueroa, R. Flauger, G. Nardini, M. Peloso, M. Pieroni, A. Ricciardone, and G. Tasinato, J. Cosmol. Astropart. Phys. 11 (2019) 017.
[97] G. Gogoberidze, T. Kahniashvili, and A. Kosowsky, Phys. Rev. D **76**, 083002 (2007).